



SIM-HOM (version 1.0): a Mechanistic Module for the 1 formation of highly oxygenated organic molecules from 2 Isoprene, Monoterpene and Sesquiterpene evaluated with 3 **ADCHAM (version 1.0)** 4 5 Liwen Yang<sup>1</sup>, Wei Nie<sup>1, 2, \*</sup>, Mikael Ehn<sup>3</sup>, Chao Yan<sup>1, 2, 4</sup>, Lubna Dada<sup>5</sup>, Yuliang Liu<sup>1, 2</sup>, 6 Pontus Roldin<sup>6</sup> and Aijun Ding<sup>1, 2</sup> 7 8 <sup>1</sup> Joint International Research Laboratory of Atmospheric and Earth System Sciences, School of Atmospheric Sciences, Nanjing University, Nanjing 210023, China 10 <sup>2</sup> National Observation and Research Station for Atmospheric Processes and 11 Environmental Change in Yangtze River Delta, Nanjing 210023, China 12 <sup>3</sup> Institute for Atmospheric and Earth System Research/Physics, Faculty of Science, 13 University of Helsinki, Helsinki 00014, Finland 14 <sup>4</sup> Nanjing-Helsinki Institute in Atmospheric and Earth System Sciences, Nanjing 15 University, Nanjing 210023, China 16 <sup>5</sup> Laboratory of Atmospheric Chemistry, Paul Scherrer Institute, 5232 Villigen, 17 Switzerland 18 <sup>6</sup> Division of Combustion Physics, Department of Physics, Lund University, P. O. Box 19 118SE-221 00 Lund, Sweden 20 \*Correspondence: Wei Nie (niewei@nju.edu.cn) 21





#### Abstract

2324

25

26

27

28

29

30

31

32

33

34

35

36

37

38

39

40

41

42

43

Biogenic volatile organic compounds (BVOCs), including isoprene, monoterpenes, and sesquiterpenes, are emitted in large quantities and play a critical role in atmospheric chemistry. They contribute to the formation of highly oxygenated organic molecules (HOM), which are essential for new particle formation (NPF) and secondary organic aerosol (SOA) formation. However, current models often oversimplify the oxidation pathways of these compounds, leading to inaccuracies in predicting HOM composition and concentrations. To address this gap, we developed a mechanistic module, SIM-HOM (Sesquiterpene, Isoprene and Monoterpene-derived HOM mechanism), based on Master Chemical Mechanism (MCM), that explicitly incorporates autoxidation processes, detailed fragmentation pathways, and RO2-RO2 interactions for isoprene, monoterpene, and sesquiterpenes. The updated module was validated using experimental data from the Cosmics Leaving OUtdoor Droplets (CLOUD) chamber, demonstrating substantial improvements in simulating HOM concentrations under various conditions. Specifically, it significantly improves the simulation of highly oxidized isoprene products, resolves discrepancies in monoterpene-derived HOM distributions, and provides the first comprehensive parameterization of sesquiterpene oxidation products. The model also captures the HOM formation under mixed precursor conditions. These advancements underscore the importance of incorporating detailed molecular-level reaction mechanisms into atmospheric models. Future work should focus on refining branching ratios for critical reactions and investigating the influence of temperature and nitrogen oxides on HOM formation, and expanding the mechanism to include additional BVOC classes. Our findings provide a robust foundation for improving global atmospheric simulations of SOA formation and climate interactions.

444546

47

48

49

50

51

52

53

54

55

56

57

58

59

60 61

62

63

64

# 1.introduction

The continental boundary layer is profoundly influenced by biogenic volatile organic compounds (BVOC) emitted by vegetation. BVOC encompass diverse compounds, including isoprene, terpenes, and related species, with specific types varying by vegetation type and environmental conditions. The global annual emission flux of isoprene (C<sub>5</sub>H<sub>8</sub>) reaches up to 594 Tg, while monoterpenes (C<sub>10</sub>H<sub>16</sub>) are emitted approximately 95 Tg annually, sustaining mixing ratio from parts per billion (ppb) levels ppb to hundreds of parts per trillion (ppt). Collectively, isoprene and monoterpenes contribute about 80% of total BVOC emissions (Sindelarova et al., 2014). Sesquiterpenes, such as β-caryophyllene, are emitted around 20 Tg annually and are highly reactive compounds with a C15 skeleton. These BVOCs react rapidly with atmospheric oxidants, including hydroxyl radicals (OH), ozone (O<sub>3</sub>), and nitrate radicals (NO<sub>3</sub>), producing low-volatility oxygenated vapors. Among these, highly oxygenated organic molecules (HOM), are particular important as they significantly contribute to particle nucleation(Kirkby et al., 2016; Riccobono et al., 2014; Lehtipalo et al., 2018), growth(Simon et al., 2020; Stolzenburg et al., 2018; Trostl et al., 2016), and secondary organic aerosol (SOA) formation(Ehn et al., 2014; Nie et al., 2022; Liu et al., 2023).

Peroxy radicals (RO<sub>2</sub>) are critical intermediates in the atmospheric oxidation of BVOC and play a central role in the formation of HOM. Under typical atmospheric conditions, a subset of RO<sub>2</sub> are produced by the oxidation of monoterpenes and sesquiterpenes by O<sub>3</sub> or OH can undergo rapid autoxidation during which internal H-shift and subsequent O<sub>2</sub> additions lead to the formation of

66

67

68 69

70

71

72

73

74

75

76

77

78

79

80

81

82

83

84

85

86

87

88

89

90

91

92

93

94

95

96

97

98 99

100

101

102

103

104

105

106

107

108





multifunctional, low-volatility compounds(Iyer et al., 2021; Berndt et al., 2016; Shen et al., 2022; Richters et al., 2016b). The autoxidation rate is strongly sensitive to molecular structure, varying by several orders of magnitude depending on functional groups, and shows significant positive temperature dependence(Crounse et al., 2013; Praske et al., 2018; Moller et al., 2016; Jorgensen et al., 2016; Knap and Jorgensen, 2017; Otkjaer et al., 2018). Concurrently, autoxidation competes with bimolecular reactions involving NO<sub>x</sub>, HO<sub>2</sub>, and other RO<sub>2</sub>. The RO<sub>2</sub>-HO<sub>2</sub> reaction typically leads to the formation of hydroperoxides, which can contribute to HOM formation or undergo further reaction. Additionally, RO<sub>2</sub>-RO<sub>2</sub> can result in the formation of HOM monomers, where two RO<sub>2</sub> react to produce two new molecules, often with one less oxygen atom than their precursors. RO<sub>2</sub>-RO<sub>2</sub> reactions can also form HOM dimers(Heinritzi et al., 2020; Berndt et al., 2018), which are less volatile than HOM monomers and play a pivotal role in NPF and SOA formation. The influence of nitrogen oxides (NO<sub>x</sub>) on HOM formation is complex: NO exhibits a nonlinear effect for cyclic monoterpenes, promoting HOM formation at low concentrations but inhibiting it at higher levels(Nie et al., 2023); whereas for isoprene, HOM formation may increase with NO(Berndt et al., 2025). NO2 tends to suppress HOM formation by consuming acyl RO2. Therefore, an accurate depiction of HOM formation requires consideration of autoxidation reactions and its competition with bimolecular RO<sub>2</sub> reactions, which are influenced by atmospheric composition, temperature, and the structure of the oxidizing molecules. Studies on the HOM formation from isoprene are limited because of its smaller molecular weight (Shen et al., 2024; Zhao et al., 2021; Wang et al., 2018; Xu et al., 2021; Curtius et al., 2024; Nie et al., 2022; Liu et al., 2021). It can suppress HOM formation by scavenging large RO2 radicals formed from the oxidation of other VOCs(Heinritzi et al., 2020; Mcfiggans et al., 2019).

Insights into HOM formation mechanisms have highlighted the need to quantify their roles under varying atmospheric conditions. This has made possible by recent experimental advances, which have driven the development of numerical models primarily targeting HOM mechanisms from monoterpenes. Computationally efficient model like the radical two-dimensional Volatility Basic Set (radical-VBS) by Schervish et al(Schervish and Donahue, 2020; Schervish et al., 2024) and CRI-HOM (Weber et al., 2020) have been implemented in some large-scale models. These frameworks are designed to represent the overall formation and partitioning behavior of HOM using parameterized volatility distributions and oxidation pathways, rather than explicitly tracking individual molecules. While grounded in mechanistic understanding, their simplified representation may omit potential important aspects of chemical complexity, such as the role of specific RO2 reaction pathways or the molecular identity of condensing vapors. Conversely, quasi-explicit approaches, such as the method by Roldin et al., 2019), provide detailed autoxidation chemistry but lack comprehensive descriptions of fragmentation products. For isoprene oxidation mechanisms, comprehensive models like the Master Chemical Mechanism (MCM)(Jenkin et al., 2015) and Caltech isoprene mechanisms (Wennberg et al., 2018) incorporate detailed representations of isoprene chemistry, consisting of hundreds of species (up to 602 in MCMv3.3.1 and 404 in the Caltech mechanism) and approximately 1000 reactions. While these existing models emphasize radical budget, carbon cycling and SOA contributions, they often do not resolve the specific HOM formation or accretion products in detail, due to their limited parameterizations. Sesquiterpenes, though often omitted from current models, can exhibit HOM yields of around 2% (Richters et al., 2016a; Jokinen et al., 2016) under laboratory conditions. Given their 15-carbon structure, the resulting oxidation products are lower volatile than those from smaller VOCs, allowing even modest

https://doi.org/10.5194/egusphere-2025-3818 Preprint. Discussion started: 18 November 2025 © Author(s) 2025. CC BY 4.0 License.





HOM yields to contribute efficiently to particle-phase mass and new particle growth.

110 Building upon these foundational studies, this study develops a unified and mechanistically detailed 111 mechanism, SIM-HOM (Sesquiterpene, Isoprene, and Monoterpene-derived HOM mechanism) that extends HOM modeling to include not only monoterpenes and isoprene, but also sesquiterpenes, an 112 113 often overlooked yet potentially important contributor due to their low volatility oxidation products(Dada et al., 2023). The model incorporates autoxidation and interactions among RO<sub>2</sub> 114 115 radicals from various VOCs, enabling a more comprehensive representation of HOM formation 116 under atmospherically relevant conditions. Section 2 details the model development based on 117 existing gas-phase chemical mechanisms and theoretical studies. Section 3 discusses the model 118 validation using the experiment data from Cosmics Leaving Outdoor Droplets (CLOUD) chamber, and section 4 summarizes this study and provides recommendations for future research. 119

#### 2. Mechanism development

120

121

122

123

124

125

126

127

128

129

130 131

132

133

The mechanism developed in this study is primarily based on the MCM framework, chosen for its comprehensive representation of organic compounds degradation in the troposphere and its ability to incorporate a wide range of atmospheric chemical reactions with detailed kinetic and mechanistic data. Within its framework, the gas-phase chemistry of isoprene was refined using updates from the Caltech isoprene mechanism, focusing on the autoxidation pathway and HOM formation. Monoterpene oxidation was addressed using modifications from the Peroxy Radical Autoxidation Mechanism (PRAM), emphasizing fragmentations and ester formation as an accretion product. For sesquiterpenes, a dedicated module was developed, leveraging both theoretical and experimental data to represent its distinctive chemical pathways to HOM formation. Additionally, we incorporated detailed interactions between different RO<sub>2</sub> species, including dimer formation. Figure 1 illustrates the primary framework of this mechanism, with specific attention to the roles of unimolecular and bimolecular reactions in driving HOM production. Detailed modifications to the base mechanism are described in the following sections.





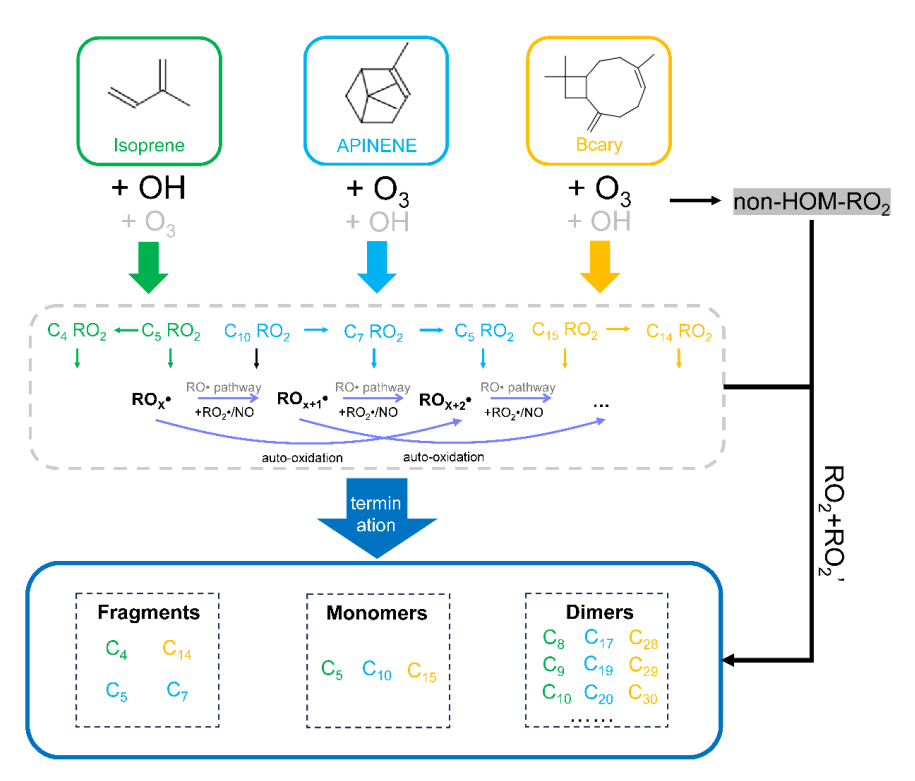


Figure 1. Schematic plot showing the mechanism of HOM formation via the oxidation of isoprene, monoterpenes and sesquiterpenes in the absence of NO<sub>x</sub>. Isoprene is primarily oxidized by OH, while monoterpenes and sesquiterpenes are primarily oxidized by O<sub>3</sub>. A small fraction of RO<sub>2</sub> can undergo autoxidation (defined as p-HOM-RO<sub>2</sub>, colored font in the figure), and the other fraction of RO<sub>2</sub> that cannot undergo autoxidation (defined as non-HOM-RO<sub>2</sub>, grey-bottomed font in the figure). p-HOM-RO<sub>2</sub> can undergo both unimolecular and bimolecular reactions, and both can form alkoxyl radicals, which can fragment or isomerize. For the dimer formation, we only consider them from RO<sub>2</sub>-RO<sub>2</sub> reactions between p-HOM-RO<sub>2</sub> and non-HOM-RO<sub>2</sub>.

#### 2.1 Extension of Isoprene Oxidation Mechanism

In recent decades, significant advancements have been made in understanding the oxidation mechanisms of isoprene, due to its key role in atmospheric chemistry and its extremely high abundance in the atmosphere. As the most emitted BVOC globally, isoprene has been widely recognized as a significant SOA precursor, forming specific intermediates such as isoprene-epoxydiol (IEPOX)(Paulot et al., 2009; Nguyen et al., 2014) and methacryloyl peroxynitrate (MPAN)(Nguyen et al., 2015), in addition to highly functionalized low-volatility compounds(Krechmer et al., 2015; D'arnbro et al., 2017; Xu et al., 2021).

Accurately representing the isoprene chemistry in large-scale atmospheric models is crucial but remains challenging due to the complex reaction mechanisms. MCM, through continuous updates, provides an almost complete compilation of isoprene's degradation pathways. Additionally,





155 Wennberg et al. (2018) conducted a systematic review of current knowledge on isoprene chemistry, 156 resulting in the development of the Caltech isoprene mechanism—a detailed reaction framework 157 capable of dynamically simulating the allylic and peroxy radical systems formed when isoprene reacts with OH radicals(Wennberg et al., 2018). Compared to earlier mechanisms, the Caltech 158 159 isoprene mechanism introduces significant advancements, including the incorporation of reversible O<sub>2</sub> addition to allyl radicals, the identification of new products from 1,6-H shifts in Z-δ-OH-peroxy 160 161 radicals, and a reduced yield of C5-hydroperoxy-aldehydes (HPALD). Furthermore, it includes more 162 intramolecular H-shift processes, such as rapid peroxyl-hydroperoxyl (RO2-OOH) shifts, which 163 enhance OH recycling rates under low-nitrogen conditions. Despite these advancements, MCM 164 provides a more detailed treatment of isoprene chemistry, including more comprehensive RO2-RO2 reactions and improved photolysis processes. The photolysis rate constants in MCM are calculated 165 166 by integrating light flux over specific wavelengths, enabling accurate representation of photolysis 167 under varying atmospheric conditions. In contrast, the Caltech mechanism calculates photolysis 168 rates using a simplified coefficient, 'sun', which relies on sunrise and sunset times. While effective 169 for outdoor scenarios, this approach does not adequately capture the intricacies of controlled 170 laboratory illumination, making MCM the preferred mechanism for laboratory-based simulations. 171 To exploit the strengths of both mechanisms, we integrated the MCM and Caltech isoprene 172 mechanisms in our framework. This posed significant challenges due to differences in species 173 naming conventions between the two frameworks. In the MCM, compounds are named 174 systematically based on their chemical structure and assigned a unique identifier, whereas the 175 Caltech mechanism employs a naming system based on the carbon skeleton and functional group positions. As a result, careful mapping of chemical species between the two mechanisms was 176 required to bridge these discrepancies (see Supplementary Information for details). This integrated 177 178 approach allows us to harness the complementary advantages of both mechanisms for a more robust 179 representation of isoprene chemistry. 180 Despite these improvements, the descriptions of HOM production from the oxidation of isoprene 181 remain incomplete. To address this gap, we incorporated autoxidation pathways for specific high-182 yield RO2 formed during isoprene oxidation, which are crucial intermediates in isoprene oxidation. 183 The key RO<sub>2</sub> radicals considered include those substituted with =O, -OH, and -OOH groups, which 184 originate from isoprene hydroxyperoxyl radicals (ISOPOO) and RO2 species formed following a 1,6 α-hydroxy H-shift in two Z-δ-ISOPOO isomers. The rapid H-shift reactions of these high-yield 185 186 RO2 radicals are critical, as they allow for the production of stable, low-volatility products under typical atmospheric conditions, making them particularly potent for HOM formation. 187 188 For these H-shift reactions to compete effectively with bimolecular reactions involving NO, HO<sub>2</sub>, and other RO<sub>2</sub>, unimolecular reaction rate constants need to reach approximately ~10<sup>-2</sup> s<sup>-1</sup> or higher. 189 Reported H-shift rates for these radicals cover a wide range, from  $8.2 \times 10^{-2}$  to  $3.0 \times 10^{5}$  s<sup>-1</sup> at 298 190 191 K(Moller et al., 2019), with hydroperoxides exhibiting notably faster rate. While the Caltech 192 isoprene mechanism assumes alkyl radicals predominantly fragment into smaller products, thus 193 limiting HOM formation, we introduced an oxygen addition pathway to alkyl radicals, as suggested in (Wang et al., 2018). This modification introduces a competing reaction pathway that can produce 194 195 new RO2 species, counterbalancing the dominance of fragmentation. Subsequent bimolecular 196 reactions involving these RO<sub>2</sub> species were implemented based on the work of (Jenkin et al., 2019). 197 Although OH oxidation overwhelmingly dominates the removal of isoprene from the atmosphere,





- 198 O<sub>3</sub> oxidation accounts for approximately 10% of isoprene's loss. Previous models primarily focused
- 199 on its contributions to the formation of methyl vinyl ketone (MVK), methacrolein (MACR), CH<sub>2</sub>OO
- 200 (C1 SCI), and OH, while largely neglecting its potential contribution to HOM formation. Here, we
- adopted a simplified approach similar to that of (Schervish et al., 2024), assuming that only a small
- 202 fraction of  $RO_2$  radicals are capable of undergoing autoxidation. These  $RO_2$  radicals can
- 203 subsequently participate in unimolecular or bimolecular reactions, with some contributing to the
- 204 HOM formation.

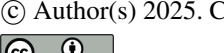
221

#### 2.2 Improvement of Monoterpene Oxidation Mechanism

- 206 Our model extends the first comprehensive Peroxy Radical Autoxidation Mechanism (PRAM)
- 207 developed by (Roldin et al., 2019). PRAM meticulously simulates the autoxidation processes of
- 208 RO<sub>2</sub> formed from monoterpene oxidation. This mechanism has demonstrated strong agreement with
- 209 observed HOM concentrations, SOA mass concentrations, and NPF in boreal forest simulations.
- 210 However, the original PRAM only considered the HOM formation pathway via monoterpene
- 211 oxidation by O<sub>3</sub> and OH. Nie et al later expanded this mechanism by incorporating NO<sub>3</sub>-initiated
- 212 oxidation pathway to the original mechanism, which mainly includes the autoxidation of
- 213 monoterpenes by NO<sub>3</sub> to form RO<sub>2</sub>; the reaction of RO<sub>2</sub> with NO<sub>3</sub> to form RO radicals (though this
- 214 pathway is negligible under most environmental conditions) and bimolecular termination reactions
- between NO<sub>2</sub> and specific RO<sub>2</sub> (e.g., acyl RO<sub>2</sub>).(Nie et al., 2023)
- 216 In this study, we further optimize the key oxidation pathways of monoterpenes, with a particular
- 217 focus on α-pinene ozonolysis, which serves as a representative case due to its atmospheric relevance
- 218 and detailed mechanistic understanding. Conventional mechanisms propose that α-pinene
- 219 ozonolysis begins with the decomposition of the primary ozonide into a carbonyl-substituted
- 220 Criegee Intermediate (CI). Three isomeric forms of this CI can undergo a 1,4 H-shift to produce
- with O<sub>2</sub> to form a RO<sub>2</sub> radical. However, under typical conditions, the isomerization of this RO<sub>2</sub>

vinyl hydroperoxide (VHP). The VHP subsequently decomposes into a vinoxy radical, which reacts

- radical is too slow to explain the observed rapid formation of HOMs. To address this, (Iyer et al.,
- 224 2021) proposed a critical solution by introducing a chemically activated ring-opening reaction of
- one of the vinoxy radicals. This reaction leads to the rapid formation of an endoperoxide and a RO<sub>2</sub>
- 226 radical with a high oxygen content (containing 8 oxygen atoms). The PRAM mechanism
- 227 incorporates this modification and further details the progressive increase in oxygen atoms within
- 228 the molecule through consecutive intramolecular RO<sub>2</sub> H-shifts and O<sub>2</sub> additions during autoxidation.
- 229 This autoxidation chain ultimately terminates through bimolecular reactions with NO, HO<sub>2</sub>, or other
- 230 RO<sub>2</sub> radicals, forming a variety of products such as alkoxy radicals, closed-shell HOM monomers,
- 231 or dimers. Once alkoxy radicals are formed, they may undergo further transformations. For example,
- they can isomerize into hydroxy-substituted alkyl radicals, which subsequently react with O<sub>2</sub> to
- 233 form new RO2 species, or they may form closed-shell HOM monomers with additional carbonyl
- 234 groups. Alternatively, they may decompose into more volatile species. A specific example of these
- fragment products includes the MCM-modeled RO<sub>2</sub> species C717O2 (an RO<sub>2</sub>), and smaller volatile
- 236 species like acetone (CH<sub>3</sub>COCH<sub>3</sub>).
- 237 In our improved model, we incorporated the C7-fragment due to recent studies indicate that early-
- 238 formed addition products retain sufficient energy to overcome transition state barriers, leading to
- 239 the formation of a significant amount of alkyl radicals with an endoperoxide group (EPO). Unlike
- 240 the traditional view that excess energy dissipates in the next O<sub>2</sub> addition step, (Yang et al., 2025)





- 241 demonstrated that EPO formation enables rearrangement pathways involving alkoxy radicals with
- epoxide groups (AOE). Their study identified that cleavage reactions from these intermediates,
- 243 which yield acetone and C<sub>7</sub> products (AE-C7), are the fastest. Furthermore, the O<sub>2</sub> addition products
- 244 (RO<sub>2</sub>) formed from AE-C7 and AE-C10 contain multiple active sites for H-shift, facilitating further
- 245 autoxidation. These findings provide key insights into the competition between unimolecular H-
- 246 shift reactions and bimolecular sinks, such as reactions with NO and HO<sub>2</sub>. Additionally, the
- 247 contribution of AE-C7 and AE-C10 derivatives explains observed peaks in mass spectrometry
- 248 corresponding to C<sub>7</sub>-HOMs.
- 249 We also incorporated RO<sub>2</sub>-Kb β-cleavage and CH<sub>2</sub>O loss to better represent the formation of C<sub>19</sub>
- 250 accretion products, like C<sub>19</sub>H<sub>28</sub>O<sub>x</sub> and C<sub>19</sub>H<sub>30</sub>O<sub>x</sub>, as observed in experiments by Berndt et al(Berndt
- et al., 2018). These products are formed through RO<sub>2</sub> self- and cross-reactions involving CH<sub>2</sub>O loss.
- Furthermore, experiments that isolated OH oxidation revealed that these C<sub>19</sub> accretion products are
- 253 not formed through pure OH-mediated processes, but rather arise specifically from O<sub>3</sub>-derived RO<sub>2</sub>
- 254 radicals (Peräkylä et al., 2023). Our updated model explicitly accounts for these distinctions,
- differentiating the contributions of OH- versus O<sub>3</sub>-derived RO<sub>2</sub> radicals in the formation of HOM
- accretion products.

### 2.3 Development of Sesquiterpene Oxidation Mechanism

- 258 Prior to our work, HOM formation from sesquiterpenes lacked a dedicated module in atmospheric
- 259 models. To address this, we developed a comprehensive framework based on the reaction pathways
- 260 proposed by (Richters et al., 2016b), integrating key processes derived from existing knowledge to
- 261 better represent the oxidation chemistry of sesquiterpenes. Given that β-caryophyllene is the only
- sesquiterpene included in MCM, our development focuses exclusively on this compound.
- 263 The ozonolysis of β-caryophyllene begins with an exothermic reaction between O<sub>3</sub> and the double
- 264 bonds of sesquiterpene molecules, forming CIs with significant excess energy. These chemically
- activated CIs can either stabilize through collisions with other molecules or undergo unimolecular
  reactions. Stable CIs may also engage in bimolecular reactions, initiating a variety of pathways that
- 267 eventually lead to HOM formation. A critical step involves the isomerization of CIs into vinyl
- 268 hydroperoxide, which further decomposes by releasing OH radicals, producing alkyl radicals as
- 269 intermediates. The alkyl radicals rapidly react with O<sub>2</sub>, forming the first generation of RO<sub>2</sub> radical.
- 270 The fate of these initial RO<sub>2</sub> radicals branches into several pathways. In one major pathway, the RO<sub>2</sub>
- 271 radical undergoes intramolecular H-shifts followed by O2 addition, resulting in new RO2 radicals
- 272 that resemble the first-generation p-HOM-RO<sub>2</sub> species observed in monoterpene ozonolysis. These
- 273 products typically include hydroperoxide (-OOH) functionalities. Alternatively, RO<sub>2</sub> radicals can
- attack the remaining double bond in the sesquiterpene structure. This process leads to the formation
- of endoperoxides and additional alkyl radicals, which subsequently react with O2 to form new RO2
- 276 radicals, though these lack the -OOH functional group. Further reaction pathways are also possible.
- 277 For instance, RO2 radicals may undergo additional intramolecular H-shifts, resulting in the
- formation of closed-shell products along with the release of OH radicals; or the subsequent O2
- 279 addition after H-shift forms a new RO<sub>2</sub>. Another pathway involves internal RO<sub>2</sub> reactions with the
- 280 remaining double bond, which can generate cyclic R radicals. These cyclic radicals then react with
- 281 O<sub>2</sub>, producing the next generation of RO<sub>2</sub> radicals.
- 282 Epoxide formation is another potential pathway, where an epoxide ring forms within the molecule,





- 283 followed by cleavage of the acyl alkoxy functionality and the expulsion of CO<sub>2</sub>. This step yields
- alkyl radicals that rapidly react with O<sub>2</sub> to form new RO<sub>2</sub> species. These RO<sub>2</sub> radicals can then enter
- 285 further autoxidation processes, involving a series of intramolecular hydrogen transfer reactions and
- successive O<sub>2</sub> additions, to produce higher-generation RO<sub>2</sub> species.
- 287 By systematically integrating these reaction pathways into our model, we developed a robust
- 288 framework to simulate HOM formation from sesquiterpene ozonolysis. The inclusion of detailed
- 289 autoxidation chemistry, along with pathways involving both -OOH and non-OOH functional group
- 290 formation, ensures a more comprehensive representation of the sesquiterpene oxidation process and
- its contribution to atmospheric HOM and SOA formation.

#### 2.4 RO<sub>2</sub> cross reactions in mixed VOC system

- 293 In real atmospheric conditions, VOC mixtures produce a variety of RO2 radicals that can react with
- each other to form RO, closed-shell monomers, or dimers. Given the vast number of RO<sub>2</sub> species in
- detailed chemical mechanisms, explicitly representing all possible cross-reactions is impractical. To
- address this, MCM uses a simplified approach, which assumes that all RO<sub>2</sub> radicals interact uniformly within a "RO<sub>2</sub> pool" at a collective rate. This is implemented using the parameter  $\Sigma$ [RO<sub>2</sub>],
- amorany wanted 1002 poor and concentre rate. This is impremented using the parameter 2[1002]
- 298 which represents the summed concentration of all RO<sub>2</sub> species. Within this framework, the total rate
- of all possible cross-reactions for a particular RO<sub>2</sub> radical is approximated as a pseudo-unimolecular 300 reaction with a rate coefficient of  $k \times \Sigma[RO_2]$ . While this simplification reduces computational
- reaction with a race coefficient of k \(^2\)[KO2]. While this simplification reduces computational
- complexity, it overlooks the specific contributions of individual RO<sub>2</sub> combinations, particularly in processes like dimer formation. The CRI-HOM model addresses dimerization by treating it as a
- simplified reaction in which one RO<sub>2</sub> radical produces half of the total dimer product. Although
- 304 efficient, this approach fails to account for differences in how specific RO<sub>2</sub> combinations influence
- 305 product distributions.

292

- 306 In our improved model, we redefine dimerization as a specific bimolecular reaction between distinct
- 307 RO<sub>2</sub> species. To reduce complexity, we focus on the interactions between two key types of RO<sub>2</sub>:
- 308 those capable of autoxidation and those that cannot undergo autoxidation (as represented in MCM).
- 309 Autoxidizable RO2 radicals, due to their higher degree of functionalization, exhibit faster
- 310 dimerization rates. Non-autoxidizable RO<sub>2</sub> radicals, which are generally present at higher
- concentrations, promote the formation of accretion products. Reactions between two autoxidizable RO<sub>2</sub> are excluded due to their extremely low concentrations, which makes their contribution to
- RO<sub>2</sub> are excluded due to their extremely low concentrations, which makes their contribution to dimer formation negligible. Likewise, reactions between two non-autoxidizable RO<sub>2</sub> are not
- 314 included due to their low propensity to form accretion products. This approach balances
- 315 computational efficiency with improved accuracy, capturing the variability in RO<sub>2</sub> reactions and
- 316 their impact on product distributions, particularly in mixed VOC systems.

#### 317 **2.5 Summary of the Model Improvements**

- We implemented several key updates to the model, focusing on the autoxidation pathway, RO<sub>2</sub>-RO<sub>2</sub>
- 319 interaction, fragmentation and termination processes. Together, these enhancements provide a more
- 320 accurate and comprehensive representation of atmospheric oxidation, enabling better simulation of
- 321 VOC oxidation and HOM formation:
- 322 (1) Expanded Autoxidation Pathways
- 323 We refined the autoxidation scheme for isoprene, monoterpenes, and sesquiterpenes by





- 324 incorporating recent experimental and theoretical advancements. Key updates include 1) High-yield
- 325 RO<sub>2</sub> autoxidation reactions for isoprene oxidation; 2) Extended formation and autoxidation
- 326 pathways for C7-RO2 species in monoterpene oxidation; 3) Integration of new autoxidation and
- 327 HOM formation processes for sesquiterpenes, building on the MCM framework.
- 328 (2) Improved RO<sub>2</sub>-RO<sub>2</sub> Interactions
- 329 For permutation reactions, we maintained MCM's computationally efficient method. However, for
- dimer formation, we moved beyond the simplified treatments used in mechanisms like CRI-HOM.
- 331 Our model explicitly parameterizes RO<sub>2</sub>-RO<sub>2</sub> interactions based on their VOC origins and
- 332 incorporates β-cleavage reactions for RO<sub>2</sub> from monoterpene ozonolysis during dimerization. This
- 333 provides a more detailed representation of dimer distributions and the behavior of mixed VOC
- 334 systems.

341

342

343 344

345

346

347

348

349 350

351

352

353

354

355

356

357

358

359360361

362

- 335 (3) Updated Fragmentation and Termination Pathways
- 336 We incorporated detailed fragmentation mechanisms for monoterpene and sesquiterpene oxidation
- 337 products, enabling more accurate predictions of experimental product distributions. Additionally,
- 338 new pathways for alkoxy radical formation and subsequent secondary RO<sub>2</sub> radicals were introduced,
- improving the representation of carbon distribution among the oxidized products.

#### 3. Model Validation Based on CLOUD Experiments

We validated the constructed model using experimental data from the Cosmic Leave Outdoor Droplet Chamber (CLOUD) at CERN. The experiments were conducted in a 26.1 cm<sup>3</sup> stainless steel chamber that can simulate diverse atmospheric conditions under well-controlled environments. Specifically, we utilized data from the CLOUD 11 campaign conducted in the fall of 2016 (Dada et al., 2023; Heinritzi et al., 2020). These experiments included oxidation of single precursors (pure isoprene,  $\alpha$ -pinene, and  $\beta$ -caryophyllene) and their mixtures, such as  $\alpha$ -pinene and isoprene, or  $\alpha$ pinene, isoprene, and β-caryophyllene. Table 1 summarizes the experimental conditions. For the mixed experiments, the precursor molar ratio (sesquiterpene: monoterpene: isoprene) was set to 1:6:50 to mimic typical BVOC emissions in the atmosphere. Most pure  $\alpha$ -pinene and  $\beta$ caryophyllene experiments were performed under dark conditions, with OH concentration of approximately  $1 \times 10^6$  cm<sup>-3</sup>, formed primarily via the BVOCs reactions with  $O_3$ . When isoprene was added, OH is predominantly consumed by isoprene, resulting in a further lower OH concentration. To increase OH concentrations, Hamamatsu UV lamps (UVH) and UV excimer lasers (UVX) were employed. No NOx was introduced in the experiments, effectively excluding NO3 oxidation pathways. The CLOUD chamber is one of the most advanced reactors for replicating atmospheric conditions, ensuring that the lifetime and reaction pathways of p-HOM-RO2 in the chamber closely resemble those in the real atmosphere. This allows p-HOM-RO2 to undergo sufficient autoxidation. The oxidation products, i.e., oxygenated organic molecules, were measured using a nitrate chemical ionization atmospheric pressure interface time-of-flight (CI-API-ToF) mass spectrometer.

Table 1. Summary of the experimental conditions used in this study. All experiments are performed at  $5^{\circ}$ C and 40% RH.

Exp	isoprene	α-pinene	Bcary	O <sub>3</sub>	UVH	UVX
Ехр	(ppt)	(ppt)	(ppt)	(ppb)		





	ID 4500	4456	0		27.5	cc	cc
isoprene	IP-4500	4456	0	0	37.5	off	off
system	IP-4500	4214	0	0	41.5	off	on
	MT-300	0	340	0	40.7	off	off
monoterpene	MT-600	0	666	0	40.2	off	off
system	MT-1200	0	1165	0	39.3	off	off
	MT-1200	0	1059	0	39.7	off	on
	SQT-1.8	0	0	1.8	47.8	off	off
Sesquiterpene	SQT-3.3	0	0	3.3	48.5	off	off
system	SQT-6.6	0	0	6.6	47.6	off	off
	SQT-6.6	0	0	6.6	48.7	on	off
Mixed	Mix I-MT300	3962	317	0	44.9	off	off
system I:	Mix I-MT600	3780	618	0	46.4	off	off
isoprene and	Mix I-MT1200	3588	1116	0	47.6	off	off
monoterpene	Mix I-MT1200	3396	1096	0	47.9	on	on
Mixed system II:	Mix II-Low	1471	303	3	45.6	on	off
isoprene,	Mix II-Medium	2695	578	7.1	45.7	on	off
monoterpene and	Mix II-High	5749	1168	15.8	44.3	on	off
sesquiterpene	Mix II-High	4578	974	15.8	44.3	on	on

 Our initial chemical mechanism did not account for deposition or condensation onto pre-existing aerosol surfaces. To address this limitation and isolate the effects of gas-phase chemistry, we coupled the chemical mechanism with the Aerosol Dynamics, gas- and particle-phase chemistry model for laboratory CHAMber studies (ADCHAM)(Roldin et al., 2014). ADCHAM integrates modules for aerosol dynamics, particle-phase chemistry, and a kinetic multilayer model to account for diffusion-limited transport between the gas phase, particle surface, and particle bulk. Once the chamber reactions reached steady-state, we simulated the HOM concentrations and compared the results with experimental data. By iteratively adjusting the rate constants for autoxidation and accretion product formation, we refined the chemical mechanism to achieve the best agreement with experimental observations.

### 3.1 Overall comparison

To assess the model's performance under varying environmental conditions, we calculated the relative error of HOM concentrations by normalizing the difference between observed and simulated concentrations. Only species with concentrations exceeding  $5 \times 10^4$  cm<sup>-3</sup> (the CI-APi-ToF detection limit) were considered. As shown in Figure 2a, the relative errors (defined as the difference between modeled and measured HOM concentrations normalized by the measurements) are illustrated as box plots. They remain close to 0 under most conditions, indicating strong agreement between model and measurements. However, in the mixed system of three VOCs (IP + MT + SQT), particularly at low VOC concentrations, larger discrepancies appear. This may be attributed to photolysis of oxidation products by UVH lamps, which is not explicitly considered in detail, leading to deviations in HOM predictions. The number of selected data points (gray dashed line) also varies

386

387

388

389

390

391

392

393

394

395

396

397

398

399

400 401

402

403

404

405

406

407

408





across different conditions, influencing error estimates.

Figure 2b compares the simulated and observed HOM concentrations across different VOC systems. The total HOM concentration varies significantly across different precursors. The isoprene system produces relatively lower HOM concentrations compared to monoterpene and sesquiterpene systems, consistent with the expected differences in oxidation pathways and HOM formation efficiency. The monoterpene system exhibits the highest HOM concentrations, particularly at higher precursor concentrations, followed by the sesquiterpene system. In mixed systems, including the isoprene-monoterpene system (Mix I) and the three-VOC mixture (Mix II), the total HOM concentration increases compared to the isoprene-only system, reflecting the contribution of monoterpenes and sesquiterpenes. The model successfully reproduces the general trends, capturing the HOM concentrations in isoprene, monoterpene, and sesquiterpene systems, as well as in mixed systems. However, overestimation is observed in some cases, particularly in low VOC concentration scenarios, as discussed earlier, likely due to incomplete representation of photolysis processes. Despite these minor deviations, the overall variations in HOM production across different VOC regimes are well reproduced.

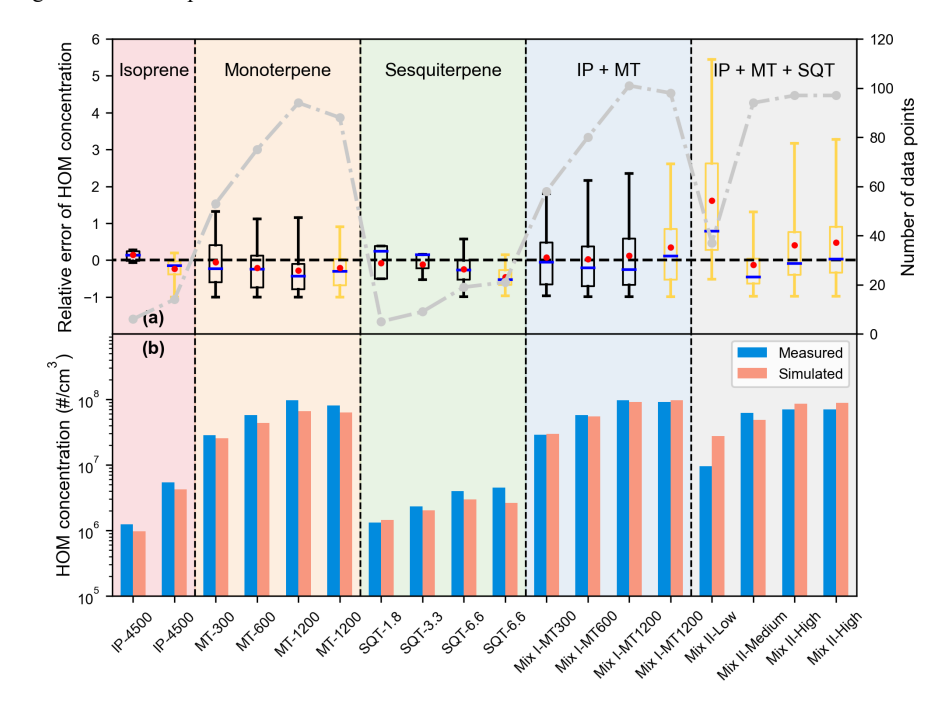


Figure 2. (a) Boxplots of relative errors and (b) comparison of simulated HOM and observations under different experimental conditions. From left to right, they represent pure isoprene, monoterpene, and sesquiterpene systems, the mixed system of isoprene, monoterpene, and the mixed system of the three VOCs. The specific experimental conditions are shown in Table 1. Boxplots represent medians, quartiles, and 5-95% percentiles, with red circles indicating the median, where the boxes are black in dark conditions and yellow in light conditions. The grey line indicates the number of HOM with higher concentration than the detection limit under each experimental

condition. Blue and outer circles indicate observed values, pink and inner circles indicate simulated





values.

#### 3.1 Isoprene system

In the pure isoprene system, the isoprene was continuously injected to maintain a concentration between 4 and 5 ppb, while O<sub>3</sub> was approximately 40 ppb, under both dark and illuminated conditions. We compared the simulation results from our improved module, MCM, the Caltech isoprene mechanism (Caltech), and their combination (MCM + Caltech). All models showed strong performance in predicting OH concentration (Fig. 3c).

Across different experimental conditions, our model exhibits significant advantages in capturing the distribution of highly oxygenated oxidation products compared to other models. For OOMs containing 5 oxygen atoms, all four models predicted concentrations notably higher than the experimental measurements (Fig. 3a and 3b), likely due to the reduced sensitivity of the NO<sub>3</sub><sup>-</sup> CI-APi-ToF mass spectrometer towards OOMs with five or fewer oxygen atoms(Riva et al., 2019). For OOMs with six or seven oxygen atoms, the MCM model significantly overestimated their concentrations, while the Caltech model underestimated them. In contrast, our model closely matched the measured data, indicating superior accuracy in simulating these oxidized species. More importantly, for OOMs containing eight or more oxygen atoms, our model was the only one capable of capturing their formation, underscoring its ability to accurately represent the complex pathways of HOM formation during isoprene oxidation.

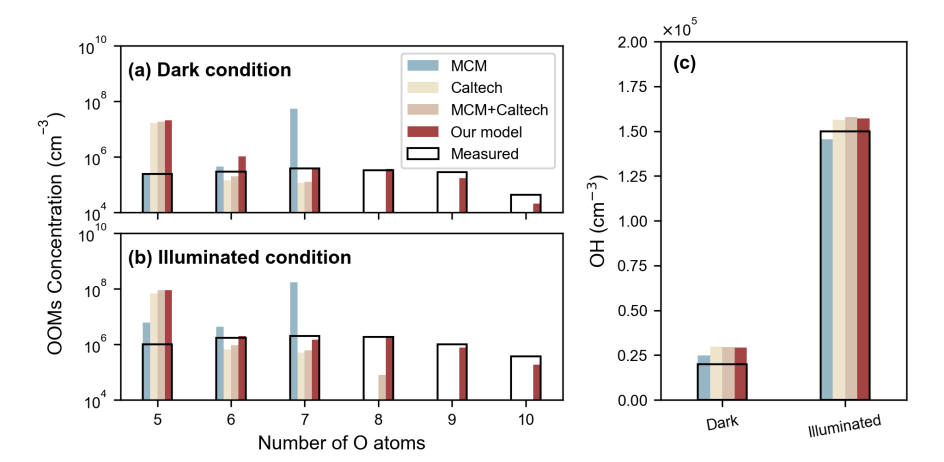


Figure 3. Comparison of measured and simulated results from four models (our improved model, MCM, Caltech, and MCM + Caltech): (a) oxidation products with varying numbers of oxygen atoms under dark conditions, (b) oxidation products under illuminated conditions, and (c) OH concentration under both dark and illuminated conditions.

Recent studies have demonstrated that isoprene-derived highly oxygenated organic molecules (IP-HOMs) play a key role in new particle formation (NPF) in the upper troposphere (Curtius et al., 2024; Shen et al., 2024; Zha et al., 2024). Our model effectively simulates the formation of HOMs, underscoring its relevance for investigating the mechanisms of NPF and subsequent particle growth. However, the observed HOM spectrum in our chamber experiments differs from that of the





atmosphere due to weak OH recycling, a consequence of the absence of  $NO_x$  and the predominantly dark or low-light experimental conditions. Atmospheric OH· levels during daytime typically remain above  $10^6$  cm<sup>-3</sup>, even in the presence of isoprene, sustaining secondary oxidation processes. As a result, atmospheric isoprene oxidation predominantly produces  $C_5H_{12}O_x$ ,  $C_5H_{11}NO_x$  and  $C_5H_{10}N_2O_x$  via second-generation OH oxidation from ISOPOOH and isoprene hydroxy nitrate(Curtius et al., 2024; Shen et al., 2024; Zha et al., 2024; Xu et al., 2021). In contrast, our experimental spectrum is dominated by  $C_5H_{8-10}O_x$  (Fig.S2), derived from the mono- and bimolecular reaction of  $RO_2$  formed directly via isoprene oxidation. A comparison of  $C_5H_{12}O_x$  concentrations with other  $C_5$  compounds (Fig.S3) further confirms that second-generation oxidation plays a minimal role in our experiments. Despite these differences, our model integrates all relevant oxidation pathways, providing a more comprehensive representation of isoprene oxidation chemistry.

#### 3.2 Monoterpene system

Fig. 4 presents the predicted oxidation products spectrum from our improved model alongside experimental measurement under different conditions. A detailed comparison with the experimental data demonstrates that our model achieves high accuracy in reproducing monoterpene oxidation processes. In particular, it effectively captures the formation of RO<sub>2</sub> radicals with 10 carbon atoms (C<sub>10</sub>-RO<sub>2</sub>) and accurately simulates their subsequent reaction pathways. Fragment simulation has traditionally been a challenge in numerical modeling. In our improved model, we incorporated C<sub>7</sub> fragments formation by incorporating recent findings on early-stage product cleavage(Yang et al., 2025). The model successfully reproduces the isomerization of C<sub>10</sub>-RO<sub>2</sub>, leading to carbon skeleton cleavage and C<sub>7</sub>-RO<sub>2</sub> formation, which undergoes autoxidation and termination to produce C<sub>7</sub>-HOMs. Furthermore, C<sub>7</sub>-RO<sub>2</sub> produces C<sub>5</sub>-RO<sub>2</sub> through RO pathway, accurately simulating key fragment products such as C<sub>5</sub>H<sub>6</sub>O<sub>7</sub>, validating the model's capability in capturing essential oxidation pathways.

Beyond accurately representing the main monomer and fragmentation product distributions, the model also exhibits significant improvements in simulating dimer formation. In particular, the enhanced formation of C<sub>7</sub>-RO<sub>2</sub> has led to an improved prediction of C<sub>17</sub>H<sub>26</sub>O<sub>9</sub> concentration, which corresponds to the most abundant dimer observed in our measurements. Additionally, the incorporation of RO<sub>2</sub>-Kb β-cleavage and CH<sub>2</sub>O loss processes have contributed to the relatively high concentrations of C<sub>19</sub>H<sub>28</sub>O<sub>9</sub> and C<sub>19</sub>H<sub>28</sub>O<sub>11</sub> dimers. Despite these advancements, the model still slightly underestimates these dimer concentrations compared to experimental observations. Several factors may contribute to this discrepancy. First, the actual yield of RO<sub>2</sub>-Kb is higher than estimated in MCM(Meder et al., 2025), leading to an underrepresentation of key dimer-forming precursors. Second, RO<sub>2</sub>-Kb cleavage products may have a higher efficiency in forming accretion products compared to other RO<sub>2</sub>, an aspect not fully accounted for in the current model. Third, additional RO<sub>2</sub> species beyond those currently considered may undergo similar cleavage reactions, contributing to dimer formation through pathways not yet incorporated (Peräkylä et al., 2023). Addressing these uncertainties by refining the branching ratios and reaction rate constants of dimerization pathways could help resolve these discrepancies and further improve the model's

478 predictive capabilities.





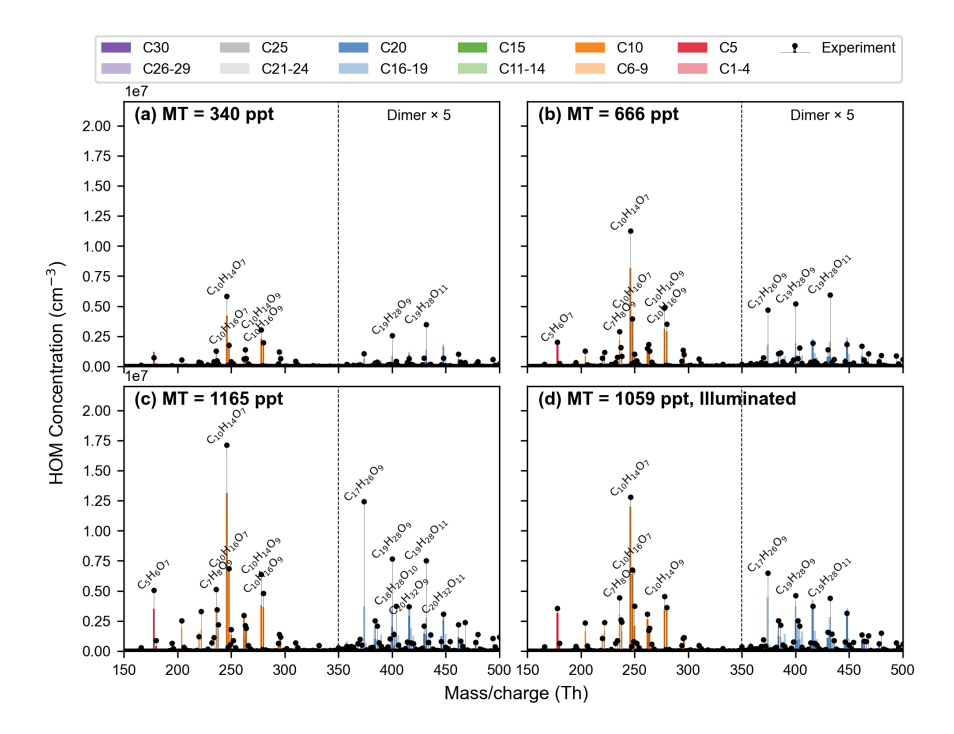


Figure 4. Comparisons between modeled and observed spectrum in  $\alpha$ -pinene oxidation experiment with (a) 340 ppt, (b) 666 ppt, (c) 1165 ppt and (d) 1059 ppt  $\alpha$ -pinene in (a-c) dark condition and (d) UV excimer laser (UVX) on. Mass/charge ratio is plotted in units of thomsons (Th) and it should be noted that the nitrate reagent ions has been removed from mass.

## 3.3 Sesquiterpene system

Fig. 5 shows that our newly developed sesquiterpene-HOM model is in strong agreement with the experimental data. During the validation process, we meticulously compared the model predictions with experimental results obtained under controlled conditions, ensuring that key chemical products - including fragmentation products, monomers, and dimers - were accurately represented. The model accurately captures the formation and transformation of these products, confirming its reliability in simulating sesquiterpene oxidation.

A key achievement of the model is its accurate prediction of C<sub>15</sub>H<sub>22</sub>O<sub>9</sub>, the most abundant HOM molecule under these experimental conditions and a critical ELVOC contributing to NPF(Dada et al., 2023). This highlights the model's ability to capture the dominant oxidation pathways of sesquiterpenes. To comprehensively describe the reaction mechanism, we incorporated an epoxide formation step, in which CO<sub>2</sub> is expelled from the acyl alkoxy functional group of the intermediate, forming an alkyl radical that rapidly reacts with O<sub>2</sub> to form an RO<sub>2</sub> radical. This modification successfully explains the observed C<sub>14</sub> fragmentation product, further improving the model's accuracy in reproducing experimental spectrum. However, while the model successfully reproduces the observed peaks for most monomers and fragments, it fails to predict C<sub>10</sub>H<sub>14</sub>O<sub>10</sub>, which is





detected at non-negligible concentrations in experiments. This discrepancy arises from the absence of reported formation pathways for this compound, suggesting that additional reaction mechanisms may need to be explored.

Regarding dimer formation, the model incorporates detailed  $RO_2$  cross-reaction pathways. While the model provides a reasonable overall prediction, it overestimates the concentrations of lower-molecular-mass dimers while underestimating the most abundant dimers, such as  $C_{29}H_{44}O_{12}$  and  $C_{29}H_{46}O_{14}$ . This suggests that refinements in the reaction rates governing dimerization processes-particular the relative contribution of  $RO_2$ - $RO_2$  from fragment  $RO_2$  are necessary to achieve better agreement with observations. Additionally, the inclusion of alternative dimerization channels, such as those involving secondary oxidation, may be required to better represent the observed dimer distribution.

Overall, the strong agreement between model predictions and experimental data indicates that our model effectively captures the fundamental oxidation mechanism governing sesquiterpene-derived HOM formation. By incorporating detailed reaction pathways and refining key parameters, the model not only reproduces observed concentration but also provides mechanistic insights into HOM formation. These advancements establish our sesquiterpene-HOM module as a valuable tool for simulating complex chemistry under atmospheric conditions.

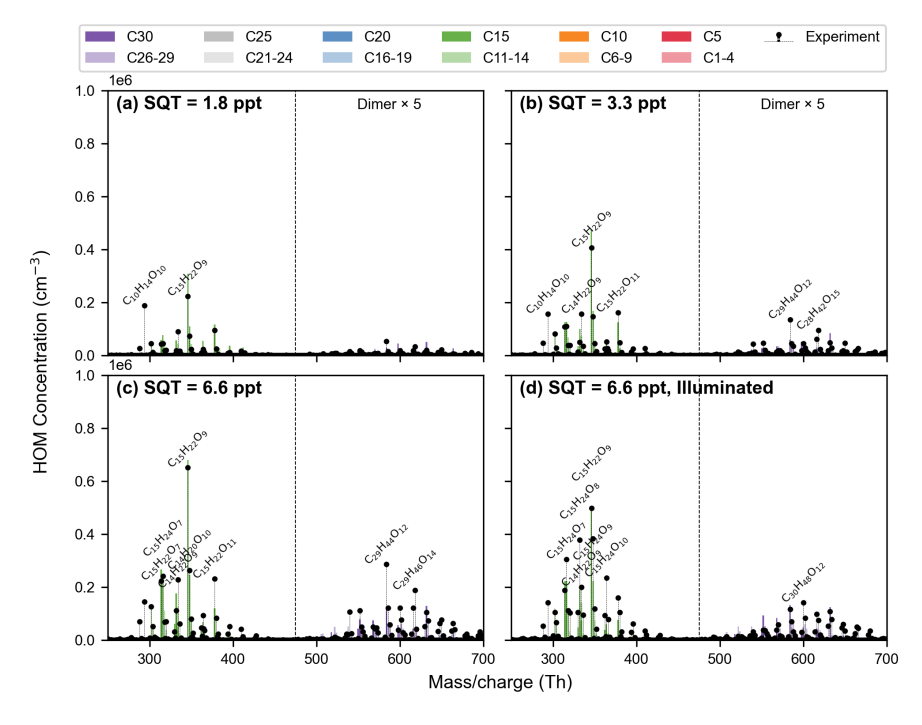


Figure 5. Comparisons between modeled and observed spectrum in  $\beta$ -caryophyllene oxidation experiment with (a) 1.8 ppt, (b) 3.3 ppt and (c-d) 6.6 ppt  $\beta$ -caryophyllene in (a-c) dark condition and (d) Hamamatsu UV lamps (UVH) on. Mass/charge ratio is plotted in units of thomsons (Th) and it should be noted that the nitrate reagent ions has been removed from mass.





#### 3.4 Mixed system

In this section, we compared the observed and simulated HOM concentrations in mixed systems under various conditions, including different VOC combinations, changes in VOC concentrations and the introduction of UV light (see Fig.S4 and Fig.S5). Across all cases, the simulations overall matched the observed HOM distributions, accurately reproducing key peaks and maintaining the expected carbon number distributions. Additionally, we analyzed the variation in HOM concentrations with different carbon numbers for four representative mixing conditions: (1) a mixture of isoprene and monoterpenes (Mix I-MT600), (2) an increased monoterpene concentration (Mix I-MT1200), (3) the introduction of UV light (Mix I-MT1200, Illuminated), and (4) the subsequent addition of sesquiterpenes (Mix II-High, Illuminated).

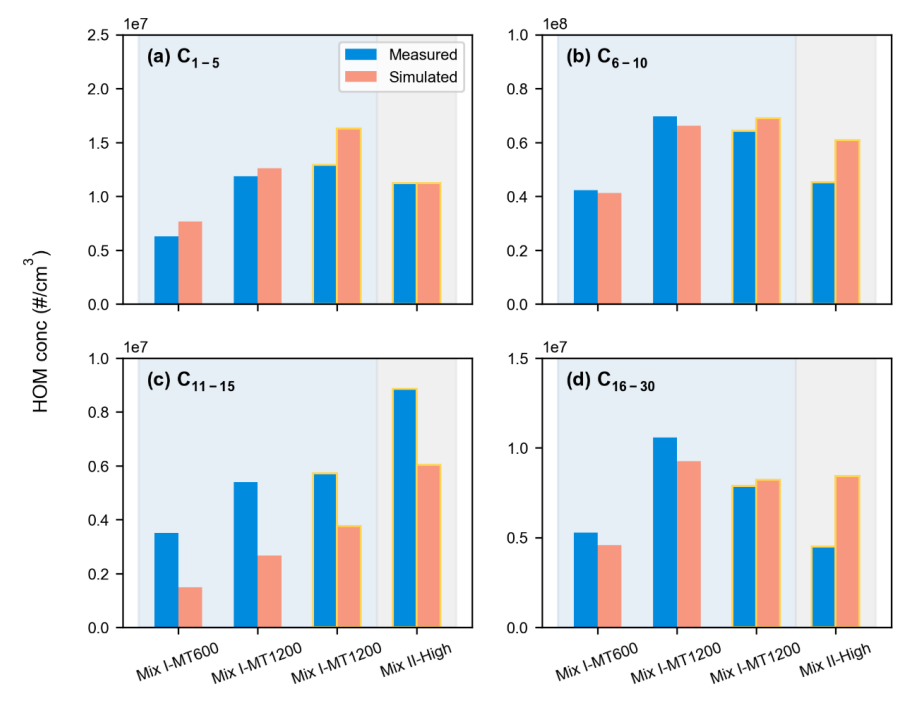


Figure 6. Experimental and simulated HOM concentration for different carbon numbers in four different mix systems (Mix I-MT600: 600 ppt  $\alpha$ -pinene + 4 ppb isoprene; Mix I-MT1200: 1200 ppt  $\alpha$ -pinene + 4 ppb isoprene; Mix I-MT1200: 1200 ppt  $\alpha$ -pinene + 4 ppb isoprene, illuminated; Mix II-High: 1200 ppt  $\alpha$ -pinene + 6 ppb isoprene + 16 ppt  $\beta$ -caryophyllene, illuminated, respectively.). Blue bars indicate observed values and pink bars indicate simulated values, where no edge color indicates dark conditions and yellow edge color indicates light conditions. The light blue background indicates the mixed system I of isoprene and monoterpenes, and the grey background indicates the mixed system II of the three VOCs. The specific experimental conditions are shown in Table 1.

In the initial isoprene-monoterpene mixture, oxidation led to a diverse range of HOMs from both

546

547

548 549

550

551

552

553

554

555556

557

558

559

560 561

562563

564 565

566

567

568

569

570

571

572

573

574

575

576

577578

579

580

581

582

583

584

585

586

587

588





C<sub>5</sub>- and C<sub>10</sub>-RO<sub>2</sub> pathways (Fig. S4a). Increasing the monoterpene concentration enhanced HOM formation, particularly for monoterpene-derived species, like C<sub>6-10</sub>- and C<sub>16-20</sub>-HOMs (from Mix I-MT600 to Mix I-MT1200, Fig.6b and 6d). The introduction of UV light shifted the HOM distribution by promoting isoprene oxidation, leading to an increase in C<sub>1-5</sub>- and C<sub>11-15</sub>-HOMs (from Mix I-MT1200 to Mix I-MT1200, illuminated, Fig. 6a and 6c) while reducing monoterpene-derived termination products in particular dimers with more than 15 carbon atoms. However, the model underestimated C<sub>11-15</sub>-HOM concentrations, likely due to an underrepresentation of cross-reaction between isoprene-derived and monoterpene-derived RO2. The addition of sesquiterpenes further altered HOM distribution, notably increasing C<sub>11-15</sub>-HOM (Fig.6c), suggesting sesquiterpenes exhibit a higher propensity for autoxidation and further amplifying these product channels. However, the significant decrease in C<sub>16-30</sub>-HOM concentration observed in three-VOC mixture, which was not reflected in the simulations (Fig.6d), could be attributed to the overestimated rate of dimer formation involving sesquiterpenes. This shift was likely driven by the competitive consumption of available RO2 radicals, which are reflected in both observations and models. Our model's ability to simulate key features—such as the redistribution of HOM classes due to competitive RO2 chemistry—demonstrates its robustness in simulating the oxidation of complex VOC mixtures. This agreement highlights the model's capability to provide mechanistic insights into HOM formation under varied atmospheric conditions.

## 4. Conclusion

In this study, we developed a novel and comprehensive mechanism, SIM-HOM (Sesquiterpene, Isoprene, and Monoterpene-derived HOM mechanism), for simulating the HOM formation from isoprene, monoterpenes, and sesquiterpenes. This mechanism incorporates intricate processes such as autoxidation and interactions among RO2 radicals derived from various BVOC, providing a more nuanced understanding of the chemical transformations leading to HOM formation. The mechanism was rigorously optimized and validated using experimental data obtained from the CLOUD chamber, thereby demonstrating its robust capability to accurately reproduce the observed concentrations of HOMs under various conditions. From an atmospheric perspective, this model is particularly valuable for understanding NPF and SOA formation. Recent studies have highlighted the nucleating potential of isoprene-derived HOMs, a process that our mechanism captures effectively. In fact, our model is the only one capable of simulating isoprene HOMs, which represents a crucial advancement in understanding NPF. Another key innovation of our work is the refinement of the monoterpene oxidation mechanism, which was already recognized as crucial in previous models, but is now further optimized to improve its representation of HOM formation. Furthermore, the inclusion of sesquiterpene-derived HOMs, which are key contributors to NPF as shown in recent literature, makes this model the first to integrate these VOCs-derived HOM in a comprehensive framework. Importantly, the improved HOM parameterization introduced here bridges the gap between detailed gas-phase chemistry and aerosol-phase processes. It is increasingly recognized that not all HOM contribute equally to SOA formation: some exhibit low volatility and can irreversibly condense onto particles, while others are semi-volatile and may evaporate on short timescales. Our framework captures these differences by resolving HOM at a near-molecular level, thereby improving predictions of both short-lived SOA and more stable aerosol mass that influences air quality and climate-relevant properties, such as cloud formation. Overall, our model significantly enhances the ability of atmospheric simulations to link specific oxidation pathways to aerosol formation outcomes, thereby offering a more mechanistic foundation for understanding and





589 predicting NPF and SOA formation across diverse environments.

However, several limitations need to be addressed. First, the model does not yet fully incorporate  $NO_x$ -related pathways. Given the significant role of  $NO_x$  in HOM formation, especially in polluted environments, refining these pathways is critical for improving predictions under high- $NO_x$  conditions. However, for isoprene and sesquiterpenes,  $NO_x$ -related mechanisms have not been explicitly included due to the lack of experimental data, highlighting a key gap in our current understanding. Additionally, the model does not yet incorporate photolysis reactions comprehensively, which can significantly alter the fate of HOMs and oxidation products under experimental conditions, such as utilizing UV lamps in the CLOUD chamber. Moreover, in the isoprene mechanism, multigenerational oxidation plays a crucial role, but its contribution to HOMs in laboratory experiments is likely lower than observed in the atmosphere. Another limitation lies in the branching ratios of key reactions, which govern the probability of different chemical pathways during autoxidation. Refining these ratios will be essential for the model's predictive capability. Expanding the mechanism to include a wider range of VOCs and their oxidation products, and considering the influence of environmental factors like temperature and atmospheric composition, will further improve its applicability under diverse conditions.

Looking forward, an important challenge lies in simplifying the mechanism for integration into computationally efficient atmospheric models, such as global or regional climate models. While our mechanism provides valuable insights into the chemical processes of HOM formation, its complexity poses a challenge for large-scale simulations. Developing simplified parameterizations that retain the key atmospheric processes while reducing computational costs will be a key step in facilitating its integration into broader atmospheric models for climate and air quality forecasting. In conclusion, this model represents a significant advancement in understanding of HOM formation and its role in atmospheric processes. However, further improvements, especially in refining NO<sub>x</sub> interactions, photolysis processes and constraining multigenerational oxidation in the isoprene system, are necessary to fully realize its potential. And efforts to simplify the mechanism for large-scale models, will be essential for broader implementation in atmospheric science and policy.

#### Code and data availability.

The ADCHAM (version 1.0) code coupled with SIM-HOM (version 1.0) mechanism used in this study is publicly available at 10.5281/zenodo.17453866. The repository also includes the model output generated in this study.

#### Author contributions.

- W.N. designed the study. L.Y performed model simulations and analyzed the data. W.N., M.E, C.Y.,
- 624 L.D, Y.L., P.R. and A.D. are acknowledged for valuable discussions. L.Y. and W.N wrote the
- 625 manuscript. M.E. and L.D. contributed to editing the manuscript.

## Competing interests.

The authors declare that they have no conflict of interest.

## Acknowledgements.





- 631 We thank CERN-CLOUD for providing experimental data. This work was supported by the
- 632 National Natural Science Foundation of China (NSFC) project (42220104006), the Jiangsu Province
- 633 Outstanding Youth Fund (BK20240067), the Natural Science Foundation of Jiangsu Province
- 634 (BK20230773), the Jiangsu Provincial Collaborative Innovation Center of Climate Change, and the
- 635 Fundamental Research Funds for the Central Universities.

- 638 Berndt, T., Hoffmann, E. H., Tilgner, A., and Herrmann, H.: Highly oxidized products from the
- 639 atmospheric reaction of hydroxyl radicals with isoprene, Nat. Commun., 16, 12, 10.1038/s41467-025-
- 640 57336-1, 2025.

Reference:

- 641 Berndt, T., Mender, B., Scholz, W., Fischer, L., Herrmann, H., Kulmala, M., and Hansel, A.: Accretion
- 642 Product Formation from Ozonolysis and OH Radical Reaction of α-Pinene: Mechanistic Insight and the
- 643 Influence of Isoprene and Ethylene, Environ. Sci. Technol., 52, 11069-11077, 10.1021/acs.est.8b02210,
- 644 2018.
- 645 Berndt, T., Richters, S., Jokinen, T., Hyttinen, N., Kurten, T., Otkjaer, R. V., Kjaergaard, H. G., Stratmann,
- 646 F., Herrmann, H., Sipila, M., Kulmala, M., and Ehn, M.: Hydroxyl radical-induced formation of highly
- oxidized organic compounds, Nat. Commun., 7, 10.1038/ncomms13677, 2016.
- 648 Crounse, J. D., Nielsen, L. B., Jorgensen, S., Kjaergaard, H. G., and Wennberg, P. O.: Autoxidation of
- 649 Organic Compounds in the Atmosphere, J. Phys. Chem. Lett., 4, 3513-3520, 10.1021/jz4019207, 2013.
- 650 Curtius, J., Heinritzi, M., Beck, L. J., Pöhlker, M. L., Tripathi, N., Krumm, B. E., Holzbeck, P.,
- Nussbaumer, C. M., Pardo, L. H., Klimach, T., Barmpounis, K., Andersen, S. T., Bardakov, R., Bohn, B.,
- 652 Cecchini, M. A., Chaboureau, J. P., Dauhut, T., Dienhart, D., Dörich, R., Edtbauer, A., Giez, A., Hartmann,
- 653 A., Holanda, B. A., Joppe, P., Kaiser, K., Keber, T., Klebach, H., Krüger, O. O., Kürten, A., Mallaun, C.,
- Marno, D., Martinez, M., Monteiro, C., Nelson, C., Ort, L., Raj, S. S., Richter, S., Ringsdorf, A., Rocha,
- 655 F., Simon, M., Sreekumar, S., Tsokankunku, A., Unfer, G. R., Valenti, I. D., Wang, N. J., Zahn, A.,
- Zauner-Wieczorek, M., Albrecht, R. I., Andreae, M. O., Artaxo, P., Crowley, J. N., Fischer, H., Harder,
- H., Herdies, D. L., Machado, L. A. T., Pöhlker, C., Pöschl, U., Possner, A., Pozzer, A., Schneider, J.,
- 658 Williams, J., and Lelieveld, J.: Isoprene nitrates drive new particle formation in Amazon's upper
- 659 troposphere, Nature, 636, 23, 10.1038/s41586-024-08192-4, 2024.
- 660 D'Arnbro, E. L., Moller, K. H., Lopez-Hilfiker, F. D., Schobesberger, S., Liu, J. M., Shilling, J. E., Lee,
- 661 B., Kjaergaard, H. G., and Thornton, J. A.: Isomerization of Second-Generation Isoprene Peroxy Radicals:
- Epoxide Formation and Implications for Secondary Organic Aerosol Yields, Environ. Sci. Technol., 51,
- 663 4978-4987, 10.1021/acs.est.7b00460, 2017.
- 664 Dada, L., Stolzenburg, D., Simon, M., Fischer, L., Heinritzi, M., Wang, M. Y., Xiao, M., Vogel, A. L.,
- 665 Ahonen, L., Amorim, A., Baalbaki, R., Baccarini, A., Baltensperger, U., Bianchi, F., Daellenbach, K. R.,
- 666 DeVivo, J., Dias, A., Dommen, J., Duplissy, J., Finkenzeller, H., Hansel, A., He, X. C., Hofbauer, V.,
- 667 Hoyle, C. R., Kangasluoma, J., Kim, C., Kürten, A., Kvashnin, A., Mauldin, R., Makhmutov, V., Marten,
- 668 R., Mentler, B., Nie, W., Petäjä, T., Quéléver, L. L. J., Saathoff, H., Tauber, C., Tome, A., Molteni, U.,
- 669 Volkamer, R., Wagner, R., Wagner, A. C., Wimmer, D., Winkler, P. M., Yan, C., Zha, Q. Z., Rissanen, M.,
- 670 Gordon, H., Curtius, J., Worsnop, D. R., Lehtipalo, K., Donahue, N. M., Kirkby, J., El Haddad, I., and
- 671 Kulmala, M.: Role of sesquiterpenes in biogenic new particle formation, Science Advances, 9,
- 672 10.1126/sciadv.adi5297, 2023.
- 673 Ehn, M., Thornton, J. A., Kleist, E., Sipila, M., Junninen, H., Pullinen, I., Springer, M., Rubach, F.,
- 674 Tillmann, R., Lee, B., Lopez-Hilfiker, F., Andres, S., Acir, I. H., Rissanen, M., Jokinen, T., Schobesberger,





- 675 S., Kangasluoma, J., Kontkanen, J., Nieminen, T., Kurten, T., Nielsen, L. B., Jorgensen, S., Kjaergaard,
- 676 H. G., Canagaratna, M., Dal Maso, M., Berndt, T., Petaja, T., Wahner, A., Kerminen, V. M., Kulmala, M.,
- 677 Worsnop, D. R., Wildt, J., and Mentel, T. F.: A large source of low-volatility secondary organic aerosol,
- 678 Nature, 506, 476-479, 10.1038/nature13032, 2014.
- 679 Heinritzi, M., Dada, L., Simon, M., Stolzenburg, D., Wagner, A. C., Fischer, L., Ahonen, L. R.,
- Amanatidis, S., Baalbaki, R., Baccarini, A., Bauer, P. S., Baumgartner, B., Bianchi, F., Brilke, S., Chen,
- 681 D. X., Chiu, R., Dias, A., Dommen, J., Duplissy, J., Finkenzeller, H., Frege, C., Fuchs, C., Garmash, O.,
- 682 Gordon, H., Granzin, M., El Haddad, I., He, X. C., Helm, J., Hofbauer, V., Hoyle, C. R., Kangasluoma,
- 683 J., Keber, T., Kim, C., Kürten, A., Lamkaddam, H., Laurila, T. M., Lampilahti, J., Lee, C. P., Lehtipalo,
- 684 K., Leiminger, M., Mai, H. J., Makhmutov, V., Manninen, H. E., Marten, R., Mathot, S., Mauldin, R. L.,
- Mentler, B., Molteni, U., Müller, T., Nie, W., Nieminen, T., Onnela, A., Partoll, E., Passananti, M., Petäjä,
- T., Pfeifer, J., Pospisilova, V., Quéléver, L. L. J., Rissanen, M. P., Rose, C., Schobesberger, S., Scholz,
- W., Scholze, K., Sipilä, M., Steiner, G., Stozhkov, Y., Tauber, C., Tham, Y. J., Vazquez-Pufleau, M.,
- Virtanen, A., Vogel, A. L., Volkamer, R., Wagner, R., Wang, M. Y., Weitz, L., Wimmer, D., Xiao, M., Yan,
- 689 C., Ye, P. L., Zha, Q. Z., Zhou, X. Q., Amorim, A., Baltensperger, U., Hansel, A., Kulmala, M., Tomé,
- 690 A., Winkler, P. M., Worsnop, D. R., Donahue, N. M., Kirkby, J., and Curtius, J.: Molecular understanding
- 691 of the suppression of new-particle formation by isoprene, Atmospheric Chemistry and Physics, 20,
- 692 11809-11821, 10.5194/acp-20-11809-2020, 2020.
- 693 Iyer, S., Rissanen, M. P., Valiev, R., Barua, S., Krechmer, J. E., Thornton, J., Ehn, M., and Kurtén, T.:
- Molecular mechanism for rapid autoxidation in  $\alpha$ -pinene ozonolysis, Nat. Commun., 12, 6,
- 695 10.1038/s41467-021-21172-w, 2021.
- 696 Jenkin, M. E., Young, J. C., and Rickard, A. R.: The MCM v3.3.1 degradation scheme for isoprene,
- 697 Atmospheric Chemistry and Physics, 15, 11433-11459, 10.5194/acp-15-11433-2015, 2015.
- 698 Jenkin, M. E., Valorso, R., Aumont, B., and Rickard, A. R.: Estimation of rate coefficients and branching
- 699 ratios for reactions of organic peroxy radicals for use in automated mechanism construction, Atmospheric
- 700 Chemistry and Physics, 19, 7691-7717, 10.5194/acp-19-7691-2019, 2019.
- 701 Jokinen, T., Kausiala, O., Garmash, O., Peräkylä, O., Junninen, H., Schobesberger, S., Yan, C., Sipilä,
- 702 M., and Rissanen, M. P.: Production of highly oxidized organic compounds from ozonolysis of β-
- 703 caryophyllene: laboratory and field measurements, Boreal Environment Research, 21, 262-273, 2016.
- 704 Jorgensen, S., Knap, H. C., Otkjaer, R. V., Jensen, A. M., Kjeldsen, M. L. H., Wennberg, P. O., and
- 705 Kjaergaard, H. G.: Rapid Hydrogen Shift Scrambling in Hydroperoxy-Substituted Organic Peroxy
- 706 Radicals, J. Phys. Chem. A, 120, 266-275, 10.1021/acs.jpca.5b06768, 2016.
- 707 Kirkby, J., Duplissy, J., Sengupta, K., Frege, C., Gordon, H., Williamson, C., Heinritzi, M., Simon, M.,
- 708 Yan, C., Almeida, J., Trostl, J., Nieminen, T., Ortega, I. K., Wagner, R., Adamov, A., Amorim, A.,
- 709 Bernhammer, A. K., Bianchi, F., Breitenlechner, M., Brilke, S., Chen, X. M., Craven, J., Dias, A., Ehrhart,
- 710 S., Flagan, R. C., Franchin, A., Fuchs, C., Guida, R., Hakala, J., Hoyle, C. R., Jokinen, T., Junninen, H.,
- Kangasluoma, J., Kim, J., Krapf, M., Kurten, A., Laaksonen, A., Lehtipalo, K., Makhmutov, V., Mathot,
- 712 S., Molteni, U., Onnela, A., Perakyla, O., Piel, F., Petaja, T., Praplan, A. P., Pringle, K., Rap, A., Richards,
- 713 N. A. D., Riipinen, I., Rissanen, M. P., Rondo, L., Sarnela, N., Schobesberger, S., Scott, C. E., Seinfeld,
- 714 J. H., Sipila, M., Steiner, G., Stozhkov, Y., Stratmann, F., Tome, A., Virtanen, A., Vogel, A. L., Wagner,
- 715 A. C., Wagner, P. E., Weingartner, E., Wimmer, D., Winkler, P. M., Ye, P. L., Zhang, X., Hansel, A.,
- 716 Dommen, J., Donahue, N. M., Worsnop, D. R., Baltensperger, U., Kulmala, M., Carslaw, K. S., and
- 717 Curtius, J.: Ion-induced nucleation of pure biogenic particles, Nature, 533, 521-526,
- 718 10.1038/nature17953, 2016.





- 719 Knap, H. C. and Jorgensen, S.: Rapid Hydrogen Shift Reactions in Acyl Peroxy Radicals, J. Phys. Chem.
- 720 A, 121, 1470-1479, 10.1021/acs.jpca.6b12787, 2017.
- 721 Krechmer, J. E., Coggon, M. M., Massoli, P., Nguyen, T. B., Crounse, J. D., Hu, W. W., Day, D. A.,
- 722 Tyndall, G. S., Henze, D. K., Rivera-Rios, J. C., Nowak, J. B., Kimmel, J. R., Mauldin, R. L., Stark, H.,
- Jayne, J. T., Sipilä, M., Junninen, H., St Clair, J. M., Zhang, X., Feiner, P. A., Zhang, L., Miller, D. O.,
- 724 Brune, W. H., Keutsch, F. N., Wennberg, P. O., Seinfeld, J. H., Worsnop, D. R., Jimenez, J. L., and
- 725 Canagaratna, M. R.: Formation of Low Volatility Organic Compounds and Secondary Organic Aerosol
- 726 from Isoprene Hydroxyhydroperoxide Low-NO Oxidation, Environ. Sci. Technol., 49, 10330-10339,
- 727 10.1021/acs.est.5b02031, 2015.
- 728 Lehtipalo, K., Yan, C., Dada, L., Bianchi, F., Xiao, M., Wagner, R., Stolzenburg, D., Ahonen, L. R.,
- 729 Amorim, A., Baccarini, A., Bauer, P. S., Baumgartner, B., Bergen, A., Bernhammer, A. K., Breitenlechner,
- 730 M., Brilke, S., Buchholz, A., Mazon, S. B., Chen, D. X., Chen, X. M., Dias, A., Dommen, J., Draper, D.
- 731 C., Duplissy, J., Ehn, M., Finkenzeller, H., Fischer, L., Frege, C., Fuchs, C., Garmash, O., Gordon, H.,
- 732 Hakala, J., He, X. C., Heikkinen, L., Heinritzi, M., Helm, J. C., Hofbauer, V., Hoyle, C. R., Jokinen, T.,
- 733 Kangasluoma, J., Kerminen, V. M., Kim, C., Kirkby, J., Kontkanen, J., Kürten, A., Lawler, M. J., Mai,
- 734 H. J., Mathot, S., Mauldin, R. L., Molteni, U., Nichman, L., Nie, W., Nieminen, T., Ojdanic, A., Onnela,
- 735 A., Passananti, M., Petäjä, T., Piel, F., Pospisilova, V., Quéléver, L. L. J., Rissanen, M. P., Rose, C.,
- 736 Sarnela, N., Schallhart, S., Schuchmann, S., Sengupta, K., Simon, M., Sipilä, M., Tauber, C., Tomé, A.,
- 737 Tröstl, J., Väisänen, O., Vogel, A. L., Volkamer, R., Wagner, A. C., Wang, M. Y., Weitz, L., Wimmer, D.,
- 738 Ye, P. L., Ylisirniö, A., Zha, Q. Z., Carslaw, K. S., Curtius, J., Donahue, N. M., Flagan, R. C., Hansel, A.,
- 739 Riipinen, I., Virtanen, A., Winkler, P. M., Baltensperger, U., Kulmala, M., and Worsnop, D. R.:
- 740 Multicomponent new particle formation from sulfuric acid, ammonia, and biogenic vapors, Science
- 741 Advances, 4, 10.1126/sciadv.aau5363, 2018.
- 742 Liu, Y. L., Liu, C., Nie, W., Li, Y. Y., Ge, D. F., Chen, L. D., Zhu, C. J., Wang, L., Zhang, Y. X., Liu, T.
- 743 Y., Qi, X. M., Wang, J. P., Huang, D. D., Wang, Z., Yan, C., Chi, X. G., and Ding, A. J.: Exploring
- 744 condensable organic vapors and their co-occurrence with PM2.5 and O3 in winter in Eastern China,
- 745 Environmental Science-Atmospheres, 3, 282-297, 10.1039/d2ea00143h, 2023.
- 746 Liu, Y. L., Nie, W., Li, Y. Y., Ge, D. F., Liu, C., Xu, Z. N., Chen, L. D., Wang, T. Y., Wang, L., Sun, P.,
- 747 Qi, X. M., Wang, J. P., Xu, Z., Yuan, J., Yan, C., Zhang, Y. J., Huang, D. D., Wang, Z., Donahue, N. M.,
- 748 Worsnop, D., Chi, X. G., Ehn, M., and Ding, A. J.: Formation of condensable organic vapors from
- anthropogenic and biogenic volatile organic compounds (VOCs) is strongly perturbed by NOx in eastern
- 750 China, Atmospheric Chemistry and Physics, 21, 14789-14814, 10.5194/acp-21-14789-2021, 2021.
- 751 McFiggans, G., Mentel, T. F., Wildt, J., Pullinen, I., Kang, S., Kleist, E., Schmitt, S., Springer, M.,
- 752 Tillmann, R., Wu, C., Zhao, D. F., Hallquist, M., Faxon, C., Le Breton, M., Hallquist, A. M., Simpson,
- 753 D., Bergstrom, R., Jenkin, M. E., Ehn, M., Thornton, J. A., Alfarra, M. R., Bannan, T. J., Percival, C. J.,
- 754 Priestley, M., Topping, D., and Kiendler-Scharr, A.: Secondary organic aerosol reduced by mixture of
- 755 atmospheric vapours, Nature, 565, 587-593, 10.1038/s41586-018-0871-y, 2019.
- 756 Meder, M., Graeffe, F., Luo, Y., Luo, J., Iyer, S., Valiev, R., Cai, R., Rissanen, M., Kurtén, T., Varelas, J.
- 757 G., Geiger, F. M., Thomson, R. J., and Ehn, M.: Selective Deuteration Reveals the Importance of Multiple
- 758 Branching Pathways in α-Pinene Autoxidation, J. Am. Chem. Soc., 147, 14131-14138,
- 759 10.1021/jacs.4c14462, 2025.
- 760 Moller, K. H., Bates, K. H., and Kjaergaard, H. G.: The Importance of Peroxy Radical Hydrogen-Shift
- 761 Reactions in Atmospheric Isoprene Oxidation, J. Phys. Chem. A, 123, 920-932,
- 762 10.1021/acs.jpca.8b10432, 2019.





- 763 Moller, K. H., Otkjær, R. V., Hyttinen, N., Kurtén, T., and Kjaergaard, H. G.: Cost-Effective
- 764 Implementation of Multiconformer Transition State Theory for Peroxy Radical Hydrogen Shift Reactions,
- 765 J. Phys. Chem. A, 120, 10072-10087, 10.1021/acs.jpca.6b09370, 2016.
- 766 Nguyen, T. B., Coggon, M. M., Bates, K. H., Zhang, X., Schwantes, R. H., Schilling, K. A., Loza, C. L.,
- 767 Flagan, R. C., Wennberg, P. O., and Seinfeld, J. H.: Organic aerosol formation from the reactive uptake
- 768 of isoprene epoxydiols (IEPOX) onto non-acidified inorganic seeds, Atmospheric Chemistry and Physics,
- 769 14, 3497-3510, 10.5194/acp-14-3497-2014, 2014.
- 770 Nguyen, T. B., Bates, K. H., Crounse, J. D., Schwantes, R. H., Zhang, X., Kjaergaard, H. G., Surratt, J.
- 771 D., Lin, P., Laskin, A., Seinfeld, J. H., and Wennberg, P. O.: Mechanism of the hydroxyl radical oxidation
- 772 of methacryloyl peroxynitrate (MPAN) and its pathway toward secondary organic aerosol formation in
- 773 the atmosphere, Phys. Chem. Chem. Phys., 17, 17914-17926, 10.1039/c5cp02001h, 2015.
- 774 Nie, W., Yan, C., Huang, D. D., Wang, Z., Liu, Y., Qiao, X., Guo, Y., Tian, L., Zheng, P., Xu, Z., Li, Y.,
- 775 Xu, Z., Qi, X., Sun, P., Wang, J., Zheng, F., Li, X., Yin, R., Dallenbach, K. R., Bianchi, F., Petäjä, T.,
- 776 Zhang, Y., Wang, M., Schervish, M., Wang, S., Qiao, L., Wang, Q., Zhou, M., Wang, H., Yu, C., Yao, D.,
- 777 Guo, H., Ye, P., Lee, S., Li, Y. J., Liu, Y., Chi, X., Kerminen, V.-M., Ehn, M., Donahue, N. M., Wang, T.,
- 778 Huang, C., Kulmala, M., Worsnop, D., Jiang, J., and Ding, A.: Secondary organic aerosol formed by
- 779 condensing anthropogenic vapours over China's megacities, Nature Geoscience, 15, 255-261,
- 780 10.1038/s41561-022-00922-5, 2022.
- 781 Nie, W., Yan, C., Yang, L., Roldin, P., Liu, Y., Vogel, A. L., Molteni, U., Stolzenburg, D., Finkenzeller,
- 782 H., Amorim, A., Bianchi, F., Curtius, J., Dada, L., Draper, D. C., Duplissy, J., Hansel, A., He, X.-C.,
- Hofbauer, V., Jokinen, T., Kim, C., Lehtipalo, K., Nichman, L., Mauldin, R. L., Makhmutov, V., Mentler,
- 784 B., Mizelli-Ojdanic, A., Petäjä, T., Quéléver, L. L. J., Schallhart, S., Simon, M., Tauber, C., Tomé, A.,
- 785 Volkamer, R., Wagner, A. C., Wagner, R., Wang, M., Ye, P., Li, H., Huang, W., Qi, X., Lou, S., Liu, T.,
- 786 Chi, X., Dommen, J., Baltensperger, U., El Haddad, I., Kirkby, J., Worsnop, D., Kulmala, M., Donahue,
- 787 N. M., Ehn, M., and Ding, A.: NO at low concentration can enhance the formation of highly oxygenated
- 788 biogenic molecules in the atmosphere, Nat. Commun., 14, 3347, 10.1038/s41467-023-39066-4, 2023.
- 789 Otkjaer, R. V., Jakobsen, H. H., Tram, C. M., and Kjaergaard, H. G.: Calculated Hydrogen Shift Rate
- 790 Constants in Substituted Alkyl Peroxy Radicals, J. Phys. Chem. A, 122, 8665-8673,
- 791 10.1021/acs.jpca.8b06223, 2018.
- Paulot, F., Crounse, J. D., Kjaergaard, H. G., Kürten, A., St Clair, J. M., Seinfeld, J. H., and Wennberg,
- 793 P. O.: Unexpected Epoxide Formation in the Gas-Phase Photooxidation of Isoprene, Science, 325, 730-
- 794 733, 10.1126/science.1172910, 2009.
- 795 Peräkylä, O., Berndt, T., Franzon, L., Hasan, G., Meder, M., Valiev, R. R., Daub, C. D., Varelas, J. G.,
- 796 Geiger, F. M., Thomson, R. J., Rissanen, M., Kurtén, T., and Ehn, M.: Large Gas-Phase Source of Esters
- 797 and Other Accretion Products in the Atmosphere, J. Am. Chem. Soc., 145, 7780-7790,
- 798 10.1021/jacs.2c10398, 2023.
- 799 Praske, E., Otkjaer, R. V., Crounse, J. D., Hethcox, J. C., Stoltz, B. M., Kjaergaard, H. G., and Wennberg,
- 800 P. O.: Atmospheric autoxidation is increasingly important in urban and suburban North America, Proc.
- 801 Natl. Acad. Sci. U. S. A., 115, 64-69, 10.1073/pnas.1715540115, 2018.
- 802 Riccobono, F., Schobesberger, S., Scott, C. E., Dommen, J., Ortega, I. K., Rondo, L., Almeida, J.,
- 803 Amorim, A., Bianchi, F., Breitenlechner, M., David, A., Downard, A., Dunne, E. M., Duplissy, J., Ehrhart,
- 804 S., Flagan, R. C., Franchin, A., Hansel, A., Junninen, H., Kajos, M., Keskinen, H., Kupc, A., Kurten, A.,
- 805 Kvashin, A. N., Laaksonen, A., Lehtipalo, K., Makhmutov, V., Mathot, S., Nieminen, T., Onnela, A.,
- 806 Petaja, T., Praplan, A. P., Santos, F. D., Schallhart, S., Seinfeld, J. H., Sipila, M., Spracklen, D. V.,





- 807 Stozhkov, Y., Stratmann, F., Tome, A., Tsagkogeorgas, G., Vaattovaara, P., Viisanen, Y., Vrtala, A.,
- 808 Wagner, P. E., Weingartner, E., Wex, H., Wimmer, D., Carslaw, K. S., Curtius, J., Donahue, N. M., Kirkby,
- 809 J., Kulmala, M., Worsnop, D. R., and Baltensperger, U.: Oxidation Products of Biogenic Emissions
- 810 Contribute to Nucleation of Atmospheric Particles, Science, 344, 717-721, 10.1126/science.1243527,
- 811 2014.
- 812 Richters, S., Herrmann, H., and Berndt, T.: Highly Oxidized RO2 Radicals and Consecutive Products
- 813 from the Ozonolysis of Three Sesquiterpenes, Environ. Sci. Technol., 50, 2354-2362,
- 814 10.1021/acs.est.5b05321, 2016a.
- 815 Richters, S., Herrmann, H., and Berndt, T.: Different pathways of the formation of highly oxidized
- 816 multifunctional organic compounds (HOMs) from the gas-phase ozonolysis of β-caryophyllene,
- 817 Atmospheric Chemistry and Physics, 16, 9831-9845, 10.5194/acp-16-9831-2016, 2016b.
- 818 Riva, M., Rantala, P., Krechmer, J. E., Peräkylä, O., Zhang, Y. J., Heikkinen, L., Garmash, O., Yan, C.,
- 819 Kulmala, M., Worsnop, D., and Ehn, M.: Evaluating the performance of five different chemical ionization
- 820 techniques for detecting gaseous oxygenated organic species, Atmos. Meas. Tech., 12, 2403-2421,
- 821 10.5194/amt-12-2403-2019, 2019.
- 822 Roldin, P., Eriksson, A. C., Nordin, E. Z., Hermansson, E., Mogensen, D., Rusanen, A., Boy, M.,
- 823 Swietlicki, E., Svenningsson, B., Zelenyuk, A., and Pagels, J.: Modelling non-equilibrium secondary
- 824 organic aerosol formation and evaporation with the aerosol dynamics, gas- and particle-phase chemistry
- 825 kinetic multilayer model ADCHAM, Atmospheric Chemistry and Physics, 14, 7953-7993, 10.5194/acp-
- 826 14-7953-2014, 2014.

- 827 Roldin, P., Ehn, M., Kurtén, T., Olenius, T., Rissanen, M. P., Sarnela, N., Elm, J., Rantala, P., Hao, L.,
- 828 Hyttinen, N., Heikkinen, L., Worsnop, D. R., Pichelstorfer, L., Xavier, C., Clusius, P., Öström, E., Petäjä,
- 829 T., Kulmala, M., Vehkamäki, H., Virtanen, A., Riipinen, I., and Boy, M.: The role of highly oxygenated
- 830 organic molecules in the Boreal aerosol-cloud-climate system, Nat. Commun., 10, 4370,
- 831 10.1038/s41467-019-12338-8, 2019.
- 832 Schervish, M. and Donahue, N. M.: Peroxy radical chemistry and the volatility basis set, Atmospheric
- 833 Chemistry and Physics, 20, 1183-1199, 10.5194/acp-20-1183-2020, 2020.
- 834 Schervish, M., Heinritzi, M., Stolzenburg, D., Dada, L., Wang, M. Y., Ye, Q., Hofbauer, V., Devivo, J.,
- 835 Bianchi, F., Brilke, S., Duplissy, J., El Haddad, I., Finkenzeller, H., He, X. C., Kvashnin, A., Kim, C.,
- 836 Kirkby, J., Kulmala, M., Lehtipalo, K., Lopez, B., Makhmutov, V., Mentler, B., Molteni, U., Nie, W.,
- 837 Petäjä, T., Quéléver, L., Volkamer, R., Wagner, A. C., Winkler, P., Yan, C., and Donahue, N. M.:
- 838 Interactions of peroxy radicals from monoterpene and isoprene oxidation simulated in the radical
- volatility basis set, Environmental Science-Atmospheres, 4, 740-753, 10.1039/d4ea00056k, 2024.
- 840 Shen, H. R., Vereecken, L., Kang, S. A., Pullinen, I., Fuchs, H., Zhao, D. F., and Mentel, T. F.: Unexpected
- 841 significance of a minor reaction pathway in daytime formation of biogenic highly oxygenated organic
- compounds, Science Advances, 8, 10.1126/sciadv.abp8702, 2022.
- 843 Shen, J. L., Russell, D. M., Devivo, J., Kunkler, F., Baalbaki, R., Mentler, B., Scholz, W., Yu, W. J.,
- Caudillo-Plath, L., Sommer, E., Ahongshangbam, E., Alfaouri, D., Almeida, J., Amorim, A., Beck, L. J.,
- Beckmann, H., Berntheusel, M., Bhattacharyya, N., Canagaratna, M. R., Chassaing, A., Cruz-Simbron,
- 846 R., Dada, L., Duplissy, J., Gordon, H., Granzin, M., Schute, L. G., Heinritzi, M., Iyer, S., Klebach, H.,
- Krueger, T., Kuerten, A., Lampimaeki, M., Liu, L., Lopez, B., Martinez, M., Morawiec, A., Onnela, A.,
- Peltola, M., Rato, P., Reza, M., Richter, S., Roerup, B., Sebastian, M. K., Simon, M., Surdu, M., Tamme,
- 850 Xenofontos, C., Yang, B. X., Zauner-Wieczorek, M., Zhang, J. Y., Zheng, Z. S., Baltensperger, U.,

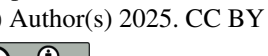
K., Thakur, R. C., Tome, A., Tong, Y. D., Top, J., Umo, N. S., Unfer, G., Vettikkat, L., Weissbacher, J.,





- 851 Christoudias, T., Flagan, R. C., El Haddad, I., Junninen, H., Moehler, O., Riipinen, I., Rohner, U.,
- 852 Schobesberger, S., Volkamer, R., Winkler, P. M., Hansel, A., Lehtipalo, K., Donahue, N. M., Lelieveld,
- 853 J., Harder, H., Kulmala, M., Worsnop, D. R., Kirkby, J., Curtius, J., and He, X. C.: New particle formation
- from isoprene under upper-tropospheric conditions, Nature, 636, 10.1038/s41586-024-08196-0, 2024.
- 855 Simon, M., Dada, L., Heinritzi, M., Scholz, W., Stolzenburg, D., Fischer, L., Wagner, A. C., Kurten, A.,
- 856 Rorup, B., He, X. C., Almeida, J., Baalbaki, R., Baccarini, A., Bauer, P. S., Beck, L., Bergen, A., Bianchi,
- 857 F., Brakling, S., Brilke, S., Caudillo, L., Chen, D. X., Chu, B. W., Dias, A., Draper, D. C., Duplissy, J.,
- 858 El-Haddad, I., Finkenzeller, H., Frege, C., Gonzalez-Carracedo, L., Gordon, H., Granzin, M., Hakala, J.,
- 859 Hofbauer, V., Hoyle, C. R., Kim, C., Kong, W. M., Lamkaddam, H., Lee, C. P., Lehtipalo, K., Leiminger,
- 860 M., Mai, H. J., Manninen, H. E., Marie, G., Marten, R., Mentler, B., Molteni, U., Nichman, L., Nie, W.,
- Ojdanic, A., Onnela, A., Partoll, E., Petaja, T., Pfeifer, J., Philippov, M., Quelever, L. L. J., Ranjithkumar,
- 862 A., Rissanen, M. P., Schallhart, S., Schobesberger, S., Schuchmann, S., Shen, J. L., Sipila, M., Steiner,
- 863 G., Stozhkov, Y., Tauber, C., Tham, Y. J., Tome, A. R., Vazquez-Pufleau, M., Vogel, A. L., Wagner, R.,
- 864 Wang, M. Y., Wang, D. S., Wang, Y. H., Weber, S. K., Wu, Y. S., Xiao, M., Yan, C., Ye, P. L., Ye, Q.,
- Zauner-Wieczorek, M., Zhou, X. Q., Baltensperger, U., Dommen, J., Flagan, R. C., Hansel, A., Kulmala,
- 866 M., Volkamer, R., Winkler, P. M., Worsnop, D. R., Donahue, N. M., Kirkby, J., and Curtius, J.: Molecular
- 867 understanding of new-particle formation from alpha-pinene between -50 and +25 °C, Atmospheric
- 868 Chemistry and Physics, 20, 9183-9207, 10.5194/acp-20-9183-2020, 2020.
- 869 Sindelarova, K., Granier, C., Bouarar, I., Guenther, A., Tilmes, S., Stavrakou, T., Müller, J. F., Kuhn, U.,
- 870 Stefani, P., and Knorr, W.: Global data set of biogenic VOC emissions calculated by the MEGAN model
- 871 over the last 30 years, Atmospheric Chemistry and Physics, 14, 9317-9341, 10.5194/acp-14-9317-2014,
- 872 2014.
- 873 Stolzenburg, D., Fischer, L., Vogel, A. L., Heinritzi, M., Schervish, M., Simon, M., Wagner, A. C., Dada,
- 874 L., Ahonen, L. R., Amorim, A., Baccarini, A., Bauer, P. S., Baumgartner, B., Bergen, A., Bianchi, F.,
- 875 Breitenlechner, M., Brilke, S., Mazon, S. B., Chen, D. X., Dias, A., Draper, D. C., Duplissy, J., Haddad,
- 876 I., Finkenzeller, H., Frege, C., Fuchs, C., Garmash, O., Gordon, H., He, X., Helm, J., Hofbauer, V., Hoyle,
- 877 C. R., Kim, C., Kirkby, J., Kontkanen, J., Kuerten, A., Lampilahti, J., Lawler, M., Lehtipalo, K.,
- 878 Leiminger, M., Mai, H., Mathot, S., Mentler, B., Molteni, U., Nie, W., Nieminen, T., Nowak, J. B.,
- 879 Ojdanic, A., Onnela, A., Passananti, M., Petaja, T., Quelever, L. L. J., Rissanen, M. P., Sarnela, N.,
- Schallhart, S., Tauber, C., Tome, A., Wagner, R., Wang, M., Weitz, L., Wimmer, D., Xiao, M., Yan, C.,
- 881 Ye, P., Zha, Q., Baltensperger, U., Curtius, J., Dommen, J., Flagan, R. C., Kulmala, M., Smith, J. N.,
- 882 Worsnop, D. R., Hansel, A., Donahue, N. M., and Winkler, P. M.: Rapid growth of organic aerosol
- nanoparticles over a wide tropospheric temperature range, Proc. Natl. Acad. Sci. U. S. A., 115, 9122-
- 884 9127, 10.1073/pnas.1807604115, 2018.
- 885 Trostl, J., Chuang, W. K., Gordon, H., Heinritzi, M., Yan, C., Molteni, U., Ahlm, L., Frege, C., Bianchi,
- 886 F., Wagner, R., Simon, M., Lehtipalo, K., Williamson, C., Craven, J. S., Duplissy, J., Adamov, A.,
- 887 Almeida, J., Bernhammer, A. K., Breitenlechner, M., Brilke, S., Dias, A., Ehrhart, S., Flagan, R. C.,
- 888 Franchin, A., Fuchs, C., Guida, R., Gysel, M., Hansel, A., Hoyle, C. R., Jokinen, T., Junninen, H.,
- 889 Kangasluoma, J., Keskinen, H., Kim, J., Krapf, M., Kurten, A., Laaksonen, A., Lawler, M., Leiminger,
- 890 M., Mathot, S., Mohler, O., Nieminen, T., Onnela, A., Petaja, T., Piel, F. M., Miettinen, P., Rissanen, M.
- P., Rondo, L., Sarnela, N., Schobesberger, S., Sengupta, K., Sipila, M., Smith, J. N., Steiner, G., Tome,
- A., Virtanen, A., Wagner, A. C., Weingartner, E., Wimmer, D., Winkler, P. M., Ye, P. L., Carslaw, K. S.,
  Curtius, J., Dommen, J., Kirkby, J., Kulmala, M., Riipinen, I., Worsnop, D. R., Donahue, N. M., and
- 894 Baltensperger, U.: The role of low-volatility organic compounds in initial particle growth in the

# https://doi.org/10.5194/egusphere-2025-3818 Preprint. Discussion started: 18 November 2025 © Author(s) 2025. CC BY 4.0 License.





- 895 atmosphere, Nature, 533, 527-531, 10.1038/nature18271, 2016.
- 896 Wang, S. N., Riva, M., Yan, C., Ehn, M., and Wang, L. M.: Primary Formation of Highly Oxidized
- Multifunctional Products in the OH-Initiated Oxidation of Isoprene: A Combined Theoretical and 897
- 898 Experimental Study, Environ. Sci. Technol., 52, 12255-12264, 10.1021/acs.est.8b02783, 2018.
- 899 Weber, J., Archer-Nicholls, S., Griffiths, P., Berndt, T., Jenkin, M., Gordon, H., Knote, C., and Archibald,
- 900 A. T.: CRI-HOM: A novel chemical mechanism for simulating highly oxygenated organic molecules
- (HOMs) in global chemistry-aerosol-climate models, Atmospheric Chemistry and Physics, 20, 10889-901
- 902 10910, 10.5194/acp-20-10889-2020, 2020.
- 903 Wennberg, P. O., Bates, K. H., Crounse, J. D., Dodson, L. G., McVay, R. C., Mertens, L. A., Nguyen, T.
- 904 B., Praske, E., Schwantes, R. H., Smarte, M. D., St Clair, J. M., Teng, A. P., Zhang, X., and Seinfeld, J.
- 905 H.: Gas-Phase Reactions of Isoprene and Its Major Oxidation Products, Chem. Rev., 118, 3337-3390,
- 906 10.1021/acs.chemrev.7b00439, 2018.
- 907 Xu, Z. N., Nie, W., Liu, Y. L., Sun, P., Huang, D. D., Yan, C., Krechmer, J., Ye, P. L., Xu, Z., Qi, X. M.,
- 908 Zhu, C. J., Li, Y. Y., Wang, T. Y., Wang, L., Huang, X., Tang, R. Z., Guo, S., Xiu, G. L., Fu, Q. Y.,
- 909 Worsnop, D., Chi, X. G., and Ding, A. J.: Multifunctional Products of Isoprene Oxidation in Polluted
- Atmosphere and Their Contribution to SOA, Geophysical Research Letters, 48, 10.1029/2020gl089276, 910
- 911
- 912 Yang, H., Raucci, U., Iyer, S., Hasan, G., Almeida, T. G., Barua, S., Savolainen, A., Kangasluoma, J.,
- 913 Rissanen, M., Vehkamäki, H., and Kurtén, T.: Molecular dynamics-guided reaction discovery reveals
- 914 endoperoxide-to-alkoxy radical isomerization as key branching point in α-pinene ozonolysis, Nat.
- 915 Commun., 16, 12, 10.1038/s41467-025-55985-w, 2025.
- 916 Yang, L., Nie, W., Ehn, M., Yan, C., Dada, L., Liu, Y., Roldin, P., & Ding, A.: SIM-HOM (Sesquiterpene,
- 917 Isoprene and Monoterpene-derived HOM mechanism). Zenodo. doi.org/10.5281/zenodo.16908325, 918
- 918 2025.
- 919 Zha, Q. Z., Aliaga, D., Krejci, R., Sinclair, V. A., Wu, C., Ciarelli, G., Scholz, W., Heikkinen, L., Partoll,
- 920 E., Gramlich, Y., Huang, W., Leiminger, M., Enroth, J., Peräkylä, O., Cai, R. L., Chen, X. M., Koenig,
- 921 A. M., Velarde, F., Moreno, I., Petäjä, T., Artaxo, P., Laj, P., Hansel, A., Carbone, S., Kulmala, M.,
- 922 Andrade, M., Worsnop, D., Mohr, C., and Bianchi, F.: Oxidized organic molecules in the tropical free
- 923 troposphere over Amazonia, Natl. Sci. Rev., 11, 11, 10.1093/nsr/nwad138, 2024.
- 924 Zhao, D. F., Pullinen, I., Fuchs, H., Schrade, S., Wu, R. R., Acir, I. H., Tillmann, R., Rohrer, F., Wildt, J.,
- 925 Guo, Y. D., Kiendler-Scharr, A., Wahner, A., Kang, S., Vereecken, L., and Mentel, T. F.: Highly
- 926 oxygenated organic molecule (HOM) formation in the isoprene oxidation by NO3 radical, Atmospheric
- 927 Chemistry and Physics, 21, 9681-9704, 10.5194/acp-21-9681-2021, 2021.

928